

AdAM: Few-Shot Image Generation via Adaptation-Aware Kernel Modulation

Yunqing Zhao, Keshigeyan Chandrasegaran, Abdollahzadeh Milad,
Chao Du, Tianyu Pang, Ruoteng Li, Henghui Ding, Ngai-Man Cheung

Abstract—Few-shot image generation (FSIG) aims to learn to generate new and diverse images given few (e.g., 10) training samples. Recent work has addressed FSIG by leveraging a GAN pre-trained on a large-scale source domain and adapting it to the target domain with few target samples. Central to recent FSIG methods are knowledge preservation criteria, which select and preserve a subset of source knowledge to the adapted model. However, a major limitation of existing methods is that their knowledge preserving criteria consider only source domain/task and fail to consider target domain/adaptation in selecting source knowledge, casting doubt on their suitability for setups of different proximity between source and target domain. Our work makes two contributions. Firstly, we revisit recent FSIG works and their experiments. We reveal that under setups which assumption of close proximity between source and target domains is relaxed, many existing state-of-the-art (SOTA) methods which consider only source domain in knowledge preserving perform no better than a baseline method. As our second contribution, we propose Adaptation-Aware kernel Modulation (AdAM) for general FSIG of different source-target domain proximity. Extensive experiments show that AdAM consistently achieves SOTA performance in FSIG, including challenging setups where source and target domains are more apart.

Index Terms—Few-Shot Learning, Generative Adversarial Networks, Generative Domain Adaptation, Generative AI, Transfer Learning, Kernel Modulation, Low-rank Approximation, Parameter-efficient Fine-tuning

1 INTRODUCTION

GENERATIVE Adversarial Networks (GANs) [1], [2], [3] have been applied to a range of important applications including image generation [3], [4], [5], image-to-image translation [6], [7], image editing [8], [9], anomaly detection [10], and data augmentation [11], [12]. However, a critical issue is that these GANs often require large-scale datasets and computationally expensive resources to achieve good performance. For example, StyleGAN [4] is trained on Flickr-Faces-HQ (FFHQ) [4] that contains 70K images, and BigGAN [2] is trained on ImageNet-1K [13]. However, in many practical applications only a few samples are available (e.g., photos of rare animal species / skin diseases, or oil paintings by artists [14]). Training a generative model is problematic in this low-data regime, where the generator often suffers from mode collapse or blurred generated images [15], [16], [17]. To address this, *few-shot image generation* (FSIG) studies the possibility of generating sufficiently diverse and high-quality images, given very limited training data (e.g., 10 samples). FSIG also attracts an increasing interest for some downstream tasks, e.g., few-shot classification [12].

1.1 Transfer Learning for FSIG

Recent works in FSIG are based on transfer learning approach [24] i.e., leveraging the prior knowledge of a GAN pretrained on a large-scale, diverse source dataset (e.g., FFHQ [4] or ImageNet-1K [13]) and adapting it to a target domain with very limited samples (e.g.,

face paintings [25]). As only very limited samples are provided to define the underlying distribution, standard fine-tuning of a pre-trained GAN suffers from mode collapse: the adapted model can only generate samples closely resembling the given few shot target samples [16], [18]. Therefore, recent works [16], [20], [21], [22], [23] have proposed to *augment* standard fine-tuning with different criteria to carefully preserve subset of source model’s knowledge into the adapted model. Various criteria has been proposed (Table 1), and these *knowledge preserving criteria* have been central in recent FSIG research. In general, these criteria aim to preserve subset of source model’s knowledge which is deemed to be useful for target-domain sample generation, e.g., improving the diversity of target sample generation.

1.2 Research Gaps to Prior Works

One major limitation of existing methods is that they consider *only* source domain in preserving subset of source model’s knowledge into the adapted model. In particular, these methods *fail to consider* target domain/adaptation task in selection of source model’s knowledge (Table 1). For example, EWC [20] applies Fisher Information [26] to select important weights entirely based on the pretrained *source* model, and it aims to preserve these selected weights regardless of the target domain in adaptation. Similar to EWC [20], CDC [16] proposes an additional constraint to preserve pairwise distances of generated images by the *source* model, and there is no consideration of target domain/adaptation. These *target/adaptation-agnostic* knowledge preserving criteria in recent works raise question regarding their suitability in different source/target domain setups. It should be noted that existing FSIG works (under very limited target samples) focus largely on setups where source and target domains are in *close proximity* (semantically) e.g., Human faces \rightarrow Baby faces [16],

- Yunqing Zhao, Keshigeyan Chandrasegaran, Abdollahzadeh Milad and Ngai-Man Cheung are with Information System Technology and Design Pillar, Singapore University of Technology and Design, 487372, Singapore.
- Chao Du and Tianyu Pang are with Sea AI Lab (SAIL), Singapore.
- Ruoteng Li was with ByteDance. Henghui Ding is with NTU, Singapore.
- Corresponding to Ngai-Man Cheung. email: ngaiman_cheung@sutd.edu.sg
- Project Page & Code: <https://yunqing-me.github.io/AdAM/>

TABLE 1: Transfer learning for few-shot image generation: Various criteria are proposed in baseline and state-of-the-art methods to augment baseline transfer learning to preserve subset of source model’s knowledge into the adapted model.

Method	Knowledge preserving criteria for FSIG	Source domain /task aware	Target domain /adaptation aware
TGAN [18]	Not available.	–	–
FreezeD [19]	Preservation of lower layers of the discriminator pre-trained on the <i>source</i> domain.	✓	✗
EWC [20]	Preservation of weights important to the <i>source</i> generative model pre-trained on the <i>source</i> domain.	✓	✗
CDC [16]	Preservation of pairwise distances of generated images by the <i>source</i> generator pre-trained on the <i>source</i> domain.	✓	✗
DCL [21]	Preservation of multilevel semantic diversity of the generated images by the <i>source</i> generator pre-trained on the <i>source</i> domain.	✓	✗
RSSA [22]	Preservation of the spatial structural knowledge of the <i>source</i> model pre-trained on the <i>source</i> domain via cross-domain consistency losses.	✓	✗
LLN [23]	Preservation of the <i>entire source</i> generator pre-trained on the <i>source</i> domain by freezing the generator and optimize the latent code during adaptation.	✓	✗
AdAM (Ours)	Preservation of kernels that are identified important in adaptation of the source model to the <i>target</i> .	✓	✓

[21], or Cars→Abandoned Cars [16], [21]. It is unclear about their performance when source/target domains are more apart (e.g., FFHQ (Human faces) [4] → AFHQ (Animal faces) [5]).

1.3 Our Contributions

In this paper, we take an important step to address these research gaps for FSIG. Specifically, our work makes two contributions. **As our first contribution**, we revisit state-of-the-art (SOTA) algorithms and their experiments. Importantly, we observe that when the close proximity assumption is relaxed in experiment setups and source/target domains are more apart, SOTA methods perform *no better* than a baseline fine-tuning method. Our observation suggests that recent methods considering only source domain/source task in knowledge preserving may not be suitable for *general* FSIG when source and target domains are more apart. To validate our claims, we introduce additional experiments with different source/target domains, analyze their proximity qualitatively and quantitatively, and examine existing methods under a unified framework.

Informed by our analysis, **as our second contribution**, we propose Adaptation-Aware kernel Modulation (AdAM) to address general FSIG of different source/target domain proximity. In marked contrast to existing works which preserve knowledge important to *source* task, AdAM aims to preserve a subset of source model’s knowledge that are important to the *target* domain and the *adaptation* task. Specifically, we propose an Importance Probing (IP) algorithm to identify kernels that encode important knowledge for adaptation to the target domain. Then, we preserve the knowledge of these kernels using a parameter-efficient *rank-constrained Kernel Modulation* (KML) during adaptation. We conduct extensive experiments to show that our proposed method consistently achieves SOTA performance across source/target domains of different proximity, including challenging setups when source/target domains are more apart. **Our main contributions are summarized as follows:**

- We revisit existing FSIG methods and experiment setups. Our study uncovers issues with existing methods when applied to source/target domains of different proximity.
- We propose Adaptation-Aware kernel Modulation (AdAM) for FSIG. Our method consistently achieves state-of-the-art performance both visually and quantitatively across source/target domains with different proximity.

2 RELATED WORKS

2.1 Few-shot Image Generation

Conventional few-shot learning [27], [28] aims at learning a discriminative classifier for classification [29], [30], [31], [32], segmentation [33], [34] or detection [35], [36] tasks. Differently, FSIG [16], [20], [21], [37], [38] aims at generating new and diverse samples given extremely limited samples (e.g., 10 shots) in training. Transfer learning has been applied to FSIG. For example, **TGAN** [18] applies the simple GAN loss [1] to fine-tune all layers of both the generator and the discriminator. **FreezeD** [19] fixes a few high-resolution discriminator layers during fine-tuning. To augment and improve simple fine-tuning, more recent works focus on preserving specific knowledge from the source models. Elastic weight consolidation (**EWC**) [20] identifies important weights for the *source* model and tries to preserve these weights. Cross-domain Correspondence (**CDC**) [16] preserves pair-wise distance of generated images from the source model to alleviate mode collapse. Dual Contrastive Learning (**DCL**) [21] applies mutual information maximization to preserve multi-level diversity of the generated images by the source model. **RSSA** [22] aims to preserve the spatial structural knowledge of the generated image by the *source model*. Latent-code Learning Network (**LLN**) [23] *freezes the entire source generator* for the *source* knowledge preservation. **However**, in this work, we observe that these SOTA methods perform poorly when the source and target domains are more apart. Therefore, their proposed source knowledge preservation criteria *may not* be generalizable. Based on our analysis, we propose a target/adaptation-aware knowledge selection which is more generalizable for source/target domains with different proximity.

2.2 Image Generation with Limited Data

There is also a fair amount of work to focus on training GANs with less (but not few-shot) data, with efforts on introducing additional data augmentation methods [39], [40], regularization terms [41], [42], modifying the GAN architectures [43], [43], [44], [45]. Many of these works focus on setups with thousands of training images, e.g.: Flowers dataset [46] with 8,189 images used in [44], 10% of ImageNet-1K used in [41] and MetFaces introduced in [39]. On the other hand, FSIG with extremely few-shot data (e.g., 10) where we focus on in this work poses unique challenges. In particular, as pointed out in [16], [20], [21], severe mode collapse and loss in diversity are critical challenges that require special attention.

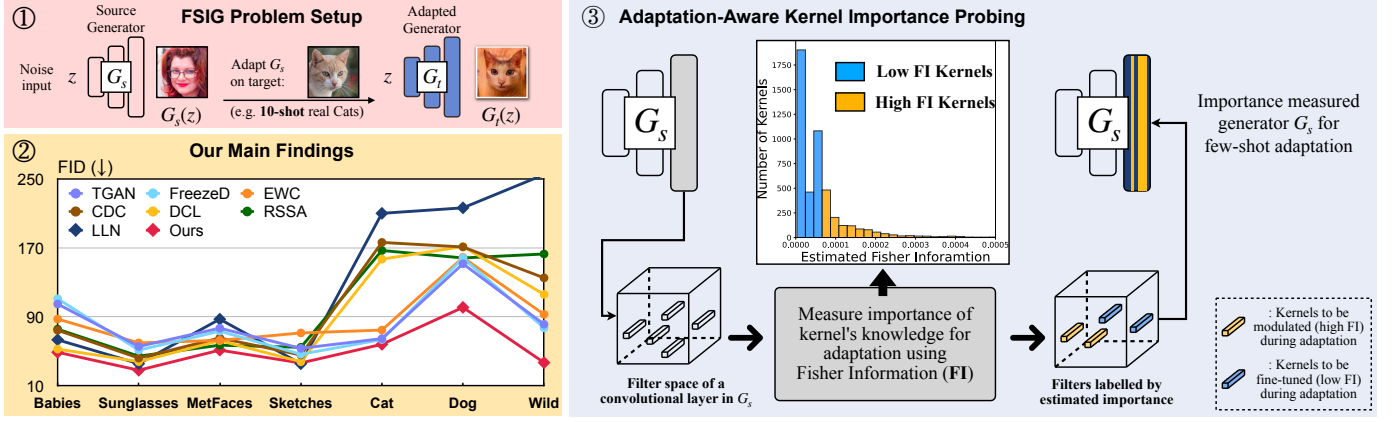


Fig. 1: **Overview and our contributions.** ①: We consider the problem of FSIG with transfer learning using very limited target samples (e.g., 10-shot). ②: • We discover that when the close proximity assumption between source-target domain is relaxed, SOTA methods (e.g. EWC [20], CDC [16], DCL [21], RSSA [22], LLN [23]) which consider only source domain/task in knowledge preserving perform *no better* than a baseline fine-tuning method (TGAN [18]) (Sec. 3). • We propose a novel Adaptation-Aware kernel Modulation (AdAM) for FSIG that achieves SOTA performance across source / target domains with different proximity (Sec. 4). ③ Schematic diagram of our proposed Importance Probing mechanism: We measure the importance of each kernel for the target domain after probing and preserve source domain knowledge that is important for target domain adaptation (Sec. 4). The same operations are applied to the discriminator.

2.3 Parameter Efficient Training

Kernel ModuLation (KML) is originally proposed in [31] for adapting the model between different modes of few-shot classification (FSC) tasks. However, due to some differences between the multimodal meta-learner in [31], and our transfer learning-based scheme, there are important differences in design choices when applying KML to our problem. First, in contrast to FSC work [31] which follows a *discriminative learning* setup, we aim to address a problem in a *generative learning* setup. Second, in FSC setup, the modulation parameters are generated during adaptation to target task with a pretrained modulation network trained on tens of thousands of few-shot tasks. So the modulation parameters are not directly learned for a target few-shot task. In contrast, in our setup, the base kernel is frozen during the adaptation, and we directly learn the modulation parameters for a target domain/task using a very limited number of samples (e.g., 10-shot). Finally, in FSC, usually source and target tasks follow the same task distribution. In fact, in implementation, even though the classes are disjoint between source and target tasks, all of them are constructed using the data from the same domain (e.g., miniImageNet [47]). However, in our setup, the source and target tasks/domains distributions could be very different (e.g., Human Faces (FFHQ) → Cats). We remark that in [44], a technique called AdaFM is introduced to update kernels. However, the underlying ideas and mechanisms of AdaFM and our KML are quite different. AdaFM is inspired from style-transfer literature [48], introduces independent scale and shift (scalar) parameters to update individual channels of kernels to manipulate their styles. On the other hand, as will be discussed in Sec. 4.2, KML updates multiple kernels in a coordinated and parameter-efficient manner. In our experiment, we also test AdaFM in few-shot setups and compare its performance with KML.

3 REVISITING FSIG THROUGH THE LENS OF SOURCE-TARGET DOMAIN PROXIMITY

In this section, we revisit existing FSIG methods (10-shot) [16], [18], [19], [20], [21] through the lens of source-target domain proximity. Specifically, we scrutinize the experimental setups of

existing FSIG methods and observe that SOTA [16], [20], [21] largely focus on adapting to target domains that are (semantically) proximal to the source domain: FFHQ → Baby Faces; FFHQ → Sunglasses; Cars → Wrecked Cars; Church → Haunted Houses. This raises the question as to whether existing source-target domain setups sufficiently represent general FSIG scenarios. Particularly, real-world FSIG applications may not contain target domains that are always proximal to the source domain (e.g.: FFHQ → Animal Faces). Motivated by this, we conduct an in-depth qualitative and quantitative analysis on source-target domain proximity where we introduce target domains that are distant from the source domain (Sec. 3.1). **Our analysis uncovers an important finding:** Under our additional setups where the assumption of close proximity between source and target domain is relaxed, existing SOTA FSIG methods [16], [20], [21] which consider only source domain/task in knowledge preserving perform *no better* than a baseline fine-tuning method [18]. We show this is due to the strong focus of existing SOTA methods in preserving source domain knowledge, thereby not being able to adapt well to distant target domains (Sec. 3.2).

3.1 Source-Target Domain Proximity Analysis

Introducing target domains with varying degrees of proximity to the source domain. In this section, we formally introduce source-target domain proximity with in-depth analysis to scrutinize existing FSIG methods under different degrees of source-target domain proximity. Following prior FSIG works [16], [18], [19], [20], [21], we use FFHQ [3] as the source domain in this analysis. We remark that existing works largely consider different types of human faces as target domains (i.e.: Babies [16], Sunglasses [16], MetFaces [39]). To relax the close proximity assumption and study *general* FSIG problems, we introduce more distant target domains namely Cat, Dog, and Wild (from AFHQ [5], consisting of ~15,000 high-quality animal face images) for our analysis.

Characterizing source-target domain proximity. Given the wide success of deep neural network features in representing meaningful semantic concepts [53], [54], [55], we visualize Inception-v3 [49] and LPIPS [50] features for source and target domains to qualitatively characterize domain proximity. Further,

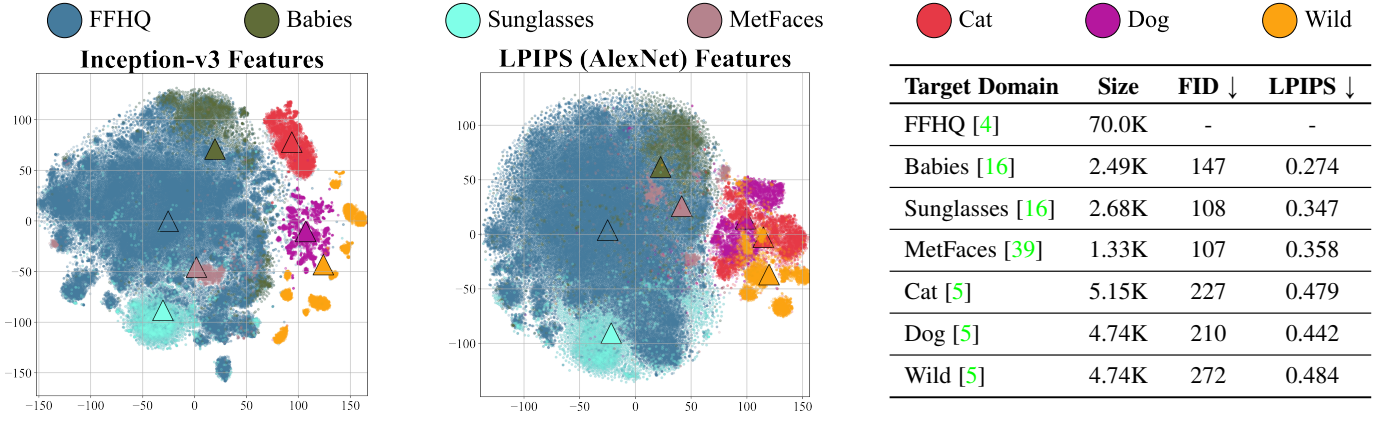


Fig. 2: Qualitative / Quantitative analysis of source-target domain proximity: We use FFHQ [3] as the source domain. We show source-target domain proximity qualitatively by visualizing Inception-v3 (Left) [49] and LPIPS (Middle) [50] – using AlexNet [51] backbone – features, and quantitatively using FID / LPIPS metrics (Right). For feature visualization, we use t-SNE [52] and show centroids (Δ) for all domains. FID / LPIPS is measured with respect to FFHQ. There are two important observations: ① Common target domains used in existing FSIG works (Babies, Sunglasses, MetFaces) are notably proximal to the source domain (FFHQ). This can be observed from the feature visualization and verified by FID / LPIPS measurements. ② We clearly show using feature visualizations and FID / LPIPS measurements that additional setups – Cat [5], Dog [5] and Wild [5] – represent target domains that are distant from the source domain (FFHQ). We remark that large FID values in this analysis are reasonable due to the distance between the source (FFHQ) and different target domains as observed from centroid distance/feature variance. The effect of limited sample size (target domains) for FID / LPIPS measurements is minimal and we include rich supportive studies in our Supplement.

we use FID [56] and LPIPS distance to quantitatively characterize source-target domain proximity. We remark that FID involves distribution estimation (first, second order moments) [56] and LPIPS computes pairwise distances (learned embeddings) [50] between source/target domains.

Results and analysis. Feature visualization and FID/ LPIPS measurement results are shown in Figure 2. Our results both qualitatively (columns 1, 2) and quantitatively (column 3) show that target domains used in existing works (Babies [3], Sunglasses [3], MetFaces [39]) are notably proximal to the source domain (FFHQ), and our additionally introduced target domains (Dog, Cat and Wild [5]) are distant from the source domain thereby relaxing the close proximity assumption in existing FSIG works.

3.2 FSIG Methods under Relaxation of Close Domain Proximity Assumption

Motivated by our analysis in Sec. 3.1, we study the performance of existing FSIG methods [16], [18], [19], [20], [21] by relaxing the close proximity assumption between source and target domains: we investigate the performance of these FSIG methods across target domains of different proximity to the source domain, which includes our additionally introduced target domains: Dog, Cat, and Wild. The FID (\downarrow) results for FFHQ \rightarrow Cat are: TGAN (simple fine-tuning) [18]: 64.68, EWC [20]: 74.61, CDC [16]: 176.21, DCL [21]: 156.82. The complete results can be found in Table 2.

We emphasize that our investigation uncovers an important finding: under setups in which the assumption of close proximity between source and target domain is relaxed, existing SOTA FSIG methods [16], [20], [21], [22], [23] perform *no better* than a baseline method [18]. This can be consistently observed in Table 2.

This finding is critical as it exposes a serious drawback of SOTA FSIG methods [16], [20], [21], [22], [23] when close domain proximity (between source and target) assumption is relaxed. We further analyse generated images from these methods and observe

that they are unable to adapt well to distant target domains due to *only considering source domain / task in knowledge preservation*. This can be clearly observed from Figure 3. We remark that TGAN (simple baseline) [18] also suffers from severe mode collapse. Given that our investigation uncovers an important problem in SOTA FSIG methods, we tackle this problem in Sec. 4. Figure 3 (last row) shows a glimpse of our proposed method.

4 ADAPTATION-AWARE KERNEL MODULATION

We focus on this question: “Given a pretrained GAN on a source domain \mathcal{S} , and a few samples from a target domain \mathcal{T} , which part of the source model’s knowledge should be preserved, and which part should be updated, during the adaptation from \mathcal{S} to \mathcal{T} ?” In contrast to SOTA FSIG methods [16], [20], [21], [22], [23], we propose an adaptation-aware FSIG that also considers the target domain/adaptation task in deciding which part of the source model’s knowledge to be preserved. In a CNN, each *kernel* is responsible for a specific part of knowledge (e.g., pattern or texture). Similar behavior is also observed for both generator [57] and discriminator [58] in GANs. Therefore, in this work, we make this knowledge preservation decision at the kernel level, i.e., *casting the knowledge preservation in FSIG to a decision problem of whether a kernel is important when adapting from \mathcal{S} to \mathcal{T}* .

Our FSIG algorithm has two main steps: (i) a lightweight *importance probing* step, and (ii) *main adaptation* step. In the first step, i.e., importance probing, we adapt the model using a parameter-efficient design to the target domain for a limited number of iterations, and during this adaptation, we measure the importance of each individual kernel for the *target domain*. The output of importance probing are decisions of importance/unimportance of individual kernels. Then, in the main adaptation step, we preserve the knowledge of important kernels and update the knowledge of unimportant kernels. The overview of the proposed system is shown in Figure 1 and the pseudocode is shown in Algorithm 1.

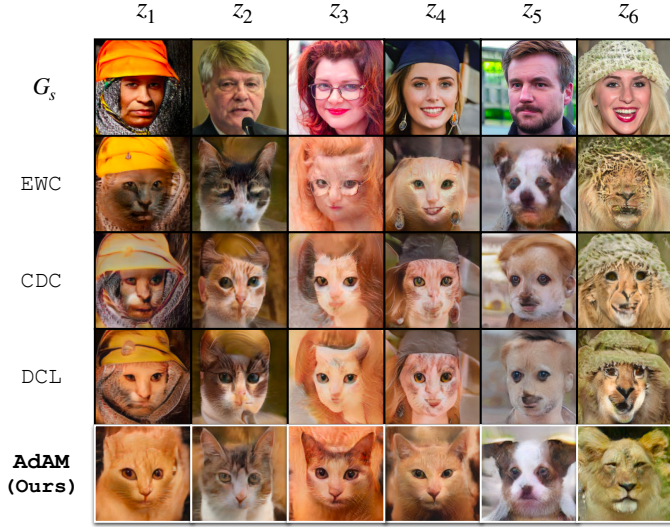


Fig. 3: G_s is the source generator (FFHQ). Adapting from the source domain (FFHQ) to distant target domains (Cat/Dog/Wild) using SOTA FSIG methods EWC [20], CDC [16], DCL [21] results in observable knowledge transfer that is incompatible to the target domain, e.g.: source task knowledge such as *Caps* (z_1, z_4, z_6), *Hair styles/color – brown* (z_2, z_5, z_6), *red-hair* (z_3), *Eyeglasses* (z_3) from FFHQ are transferred to Cat/Dog/Wild during adaptation which is not appropriate. Our method can alleviate these issues.

4.1 Importance Probing for FSIG

Our intuition for the proposed importance probing is: “*The source GAN kernels have different levels of importance for each target domain.*” For example, different subsets of kernels could be important when adapting a pretrained GAN on FFHQ to Babies [16] compared to adapting the same pretrained GAN to Cat [5]. Therefore, we aim for a knowledge preservation criterion that is target domain/adaptation-aware (a comparison is in Table 1). In order to achieve adaptation awareness, we propose a lightweight importance probing algorithm that considers adaptation from the source to the target domain. There are two important design considerations: probing under (i) extremely limited number of target data and (ii) low computation overhead.

As discussed, in this *importance probing* step, we adapt the source model to the target domain for a limited number of iterations and with a few available target samples. During this short adaptation step, we measure the importance of the kernel for the adaptation task. To measure the importance, we use Fisher information (FI) which gives the *informative knowledge* of that kernel in handling adaptation task [59]. Then, based on FI measurement, we classify kernels into important/unimportant. These kernel-level importance decisions are then used in the next step, i.e., main adaptation.

In the main adaptation step, we propose to apply *kernel modulation* to achieve restrained update for the important kernels, and *simple fine-tuning* for the unimportant kernels. As will be discussed in Sec. 4.3, the modulation is rank-constrained and has a restricted degree of freedom, therefore, it is capable to preserve the knowledge of the important kernels (also see results in Supplement). On the other hand, simple fine-tuning has a large degree of freedom for updating knowledge of the unimportant kernels. Furthermore, the rank-constrained kernel modulation is parameter-efficient, therefore, we also apply this rank-constrained kernel modulation in the probing step to determine the importance of kernels.

4.2 Kernel Modulation

The Kernel Modulation (KML) is used in the main adaptation step to preserve knowledge of important kernels in the adapted model. Furthermore, it is also used in the probing step as a parameter-efficient technique to determine importance of kernels. Specifically, we apply KML which is proposed very recently [31]. In [31], KML is proposed for multi-modal few-shot classification (FSC). In particular, in [31], KML is found to be effective for knowledge transfer between different *classification* tasks of different modes under few-shot constraints. Therefore, in our work, we apply KML for knowledge transfer between different *generation* tasks of different domains under limited target domain samples.

Specifically, in each convolutional layer of a CNN, the i^{th} kernel of that layer $\mathbf{W}_i \in \mathbb{R}^{c_{in} \times k \times k}$ is convolved with the input feature $\mathbf{X} \in \mathbb{R}^{c_{in} \times h \times w}$ to the layer to produce the i^{th} output channel (feature map) $\mathbf{Y}_i \in \mathbb{R}^{h' \times w'}$, i.e., $\mathbf{Y}_i = \mathbf{W}_i * \mathbf{X} + b_i$, where $b_i \in \mathbb{R}$ denotes the bias term. Then, KML modulates \mathbf{W}_i by multiplying it with the modulation matrix $\mathbf{M}_i \in \mathbb{R}^{c_{in} \times k \times k}$ plus an all-ones matrix $\mathbf{J} \in \mathbb{R}^{c_{in} \times k \times k}$:

$$\hat{\mathbf{W}}_i = \mathbf{W}_i \odot (\mathbf{J} + \mathbf{M}_i), \quad (1)$$

where \odot denotes the Hadamard multiplication. In Eqn. 1, using \mathbf{J} allows learning the modulation matrix in a residual format. Therefore, the modulation weights are learned as perturbations around the pretrained (and fixed) kernel which help to preserve the source knowledge. The exact pretrained kernel can also be transferred to the target model if it is optimal.

4.3 Parameter-Efficient KML via Low-rank Approximation

The baseline KML in Sec. 4.2 learns an individual modulation parameter for each coefficient of the kernel. Therefore, it could suffer from *parameter explosion* when using in recent GAN architectures (e.g., more than 58M parameters in StyleGAN-V2 [3]). To address this issue, instead of learning the modulation matrix, we learn a *low-rank* version of it [31], [60]. More specifically, for a Conv layer within CNN, with a total number of d_{out} kernels to be modulated, instead of learning $\mathbf{M} = \{\mathbf{M}_i\}_{i=1}^{d_{out}}$, we learn two proxy vectors $\mathbf{m}_1 \in \mathbb{R}^{d_{out}}$, and $\mathbf{m}_2 \in \mathbb{R}^{(c_{in} \times k \times k)}$, and construct the modulation matrix using the outer product of these vectors, i.e., $\mathbf{M} = \mathbf{m}_1 \otimes \mathbf{m}_2$. Furthermore, as we are using KML for adaptable knowledge preservation, we *freeze* the base kernel \mathbf{W}_i during adaptation. Therefore, trainable parameters are $\mathbf{m}_1, \mathbf{m}_2$.

KML reduces the number of trainable parameters significantly and has better performance in restraining the update of important kernels (results are in Supplement). An illustration of our parameter-efficient KML operations is in Figure 4.

As will be discussed in Sec. 4.4, the value of d_{out} equals to the total number of kernels in a layer (c_{out}) during the importance probing process, and for the main adaptation, it is determined by the output of our probing method (i.e., $d_{out} \leq c_{out}$).

4.4 Importance Measurement

Recall our FSIG has two main steps: (i) importance probing step (Lines 1-8 in Algorithm 1), and (ii) main adaptation step (Lines 9-21 in Algorithm 1). In probing, we also apply KML as a parameter-efficient technique to determine the importance of individual kernels. In particular, for probing, we propose to apply KML to all kernels (in both generator and discriminator) to identify which of the *modulated* kernels are important for the adaptation task. To measure the importance of the modulated kernels, we

Algorithm 1: Few-Shot Image Generation via Adaptation-Aware Kernel Modulation (AdAM)

Require: Pre-trained GAN: G_s and D_s , $iter_{probe}$, $iter_{adapt}$, threshold quantile t_h , learning rate α

Importance Probing:

- 1 Freeze all kernels $\{\mathbf{W}_i\}_{i=1}^N$ in pre-trained networks G_s , and D_s
- 2 Randomly initialize a modulation matrix \mathbf{M}_i for each kernel \mathbf{W}_i
- 3 **for** $k = 0, k++$, **while** $k < iter_{probe}$ **do**
- 4 Perform kernel modulation for all kernels using Eqn. 1 to obtain modulated weights $\hat{\mathbf{W}}$
- 5 Update $\mathbf{M} \leftarrow \mathbf{M} - \alpha \nabla_{\mathbf{M}} \mathcal{L}(G(z); \hat{\mathbf{W}}) / *$ lightweight, i.e., $iter_{probe} \ll iter_{adapt}$ $*/$
- 6 **end**
- 7 Measure the importance of each kernel \mathbf{W}_i by computing FI for the corresponding \mathbf{M}_i using Eqn. 3
- 8 Compute the index set \mathcal{A} of important kernels using quantile t_h of FI values as threshold

Main Adaptation:

- 9 **if** $j \in \mathcal{A}$ **then**
- 10 Initialize the kernel by \mathbf{W}_j and freeze the kernel, randomly initialize \mathbf{M}_j
- 11 **else**
- 12 Initialize the kernel by \mathbf{W}_j
- 13 **end**
- 14 **for** $k = 0, k++$, **while** $k < iter_{adapt}$ **do**
- 15 **if** $j \in \mathcal{A}$ **then**
- 16 Modulate kernel using Eqn. 1 to obtain modulated weights $\hat{\mathbf{W}}_j$
- 17 Update $\mathbf{M}_j \leftarrow \mathbf{M}_j - \alpha \nabla_{\mathbf{M}_j} \mathcal{L}(G(z); \hat{\mathbf{W}}_j)$
- 18 **else**
- 19 Update $\mathbf{W}_j \leftarrow \mathbf{W}_j - \alpha \nabla_{\mathbf{W}_j} \mathcal{L}(G(z); \hat{\mathbf{W}}_j)$
- 20 **end**
- 21 **end**

apply Fisher information (FI) to the modulation parameters. In our FSIG setup, for a modulated GAN with parameters Θ , Fisher information \mathcal{F} can be computed as:

$$\mathcal{F}(\Theta) = \mathbb{E} \left[-\frac{\partial^2}{\partial \Theta^2} \mathcal{L}(x|\Theta) \right], \quad (2)$$

where $\mathcal{L}(x|\Theta)$ is the binary cross-entropy loss computed using the output of the discriminator, and x includes few-shot target samples, and fake samples generated by GAN. Then, FI for a modulation matrix $\mathcal{F}(\mathbf{M}_i)$ can be computed by averaging over FI values of parameters within that matrix. As we are using the low-rank estimation to construct the modulation matrix, we can estimate $\mathcal{F}(\mathbf{M}_i)$ by FI values of the proxy vectors (i.e., \mathbf{m}_1 and \mathbf{m}_2). In particular, considering the outer product in low-rank approximation, we have $\mathbf{M}_i = ([\mathbf{m}_1^i \mathbf{m}_2^1, \dots, \mathbf{m}_1^i \mathbf{m}_2^{(c_{in} \times k \times k)}]) . \text{reshape}()$, where $|\mathbf{m}_2| = c_{in} \times k \times k$. Then we use the unweighted average of FI for parameters of \mathbf{m}_1 and \mathbf{m}_2 , proportional to their occurrence frequency in the calculation of \mathbf{M}_i , as an estimate of $\mathcal{F}(\mathbf{M}_i)$ (we discuss more details in Supplement):

$$\hat{\mathcal{F}}(\mathbf{M}_i) = \mathcal{F}(\mathbf{m}_1^i) + \frac{1}{|\mathbf{m}_2|} \sum_{j=1}^{|\mathbf{m}_2|} \mathcal{F}(\mathbf{m}_2^j). \quad (3)$$

After calculating $\hat{\mathcal{F}}(\mathbf{M}_i)$ for all modulation matrices in both generator and discriminator, we use the $t_h(\%)$ quantile of these values as a threshold to decide whether modulation of a kernel is important or unimportant for adaptation to the target domain. If the modulation of a kernel is determined to be important (during probing), the kernel is modulated using KML during the main adaptation step; otherwise, the kernel is updated using simple fine-tuning during the main adaptation. In all setups, we perform probing

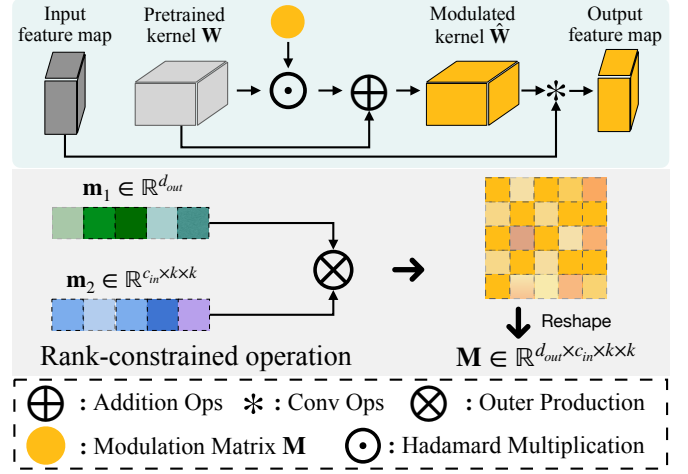
Overview: Kernel Modulation (KML) of a Conv layer


Fig. 4: **Left:** Overview of KML on Conv layer. **Right:** Parameter-efficient KML via rank-constraint operation. For a Conv kernel with size $\mathbb{R}^{c_{out} \times c_{in} \times k \times k}$, the two learnable proxy vectors $\mathbf{m}_1 \in \mathbb{R}^{d_{out}}$ and $\mathbf{m}_2 \in \mathbb{R}^{(c_{in} \times k \times k)}$ where $d_{out} \leq c_{out}$. We remark that the KML operation is parameter-efficient: For example, if the Conv kernel $\in \mathbb{R}^{512 \times 512 \times 3 \times 3}$ (which is standard in StyleGAN-V2), the number of parameters learned via KML is up to $512 + 512 \times 3 \times 3$ (when $d_{out} = c_{out}$), which is only 1/460 of the entire Conv layer.

for 500 iterations. We remark that in probing only modulation parameters $\mathbf{m}_1, \mathbf{m}_2$ are trainable, and FI is only computed on them, therefore the probing is a very lightweight step and can be performed with minimal overhead (details are in Supplement). The output of the probing step is the decision to apply kernel modulation or simple fine-tuning on individual kernels. Then, based on these decisions, the main adaptation is performed. Overall, our proposed method, AdAM, is summarized in Algorithm 1.

5 EMPIRICAL STUDIES

5.1 Implementation Details

For a fair comparison, we strictly follow prior works [16], [18], [19], [20], [21], [22], [23] in the choice of GAN architecture, source-target adaptation setups, and hyper-parameters. We use StyleGAN-V2 [3] as the GAN architecture and FFHQ as the source domain. Our experiments include setups with different source-target proximity: Babies/Sunglasses [16], MetFaces [39] and Cat/Dog/Wild (AFHQ) [5] (See Sec. 3). Adaptation is performed with 256x256 resolution, batch size 4 with initial learning rate 0.002 on a single Tesla V100 GPU. We apply importance probing and modulation on the base kernels of both the generator and the discriminator. We focus on 10-shot target adaptation setup in the main experiments, with additional setups in our analysis and ablation studies, see Sec. 6 and also Supplement.

5.2 Qualitative Results

We show generated images with our proposed AdAM along with baseline [18], [19] and SOTA methods [16], [20], [21], [22], [23] for two target domains, Babies and AFHQ-Cat with different degrees of proximity to FFHQ, before and after adaptation. The results are shown in Figure 5 top and bottom, respectively. By preserving source domain knowledge that is important for the target domain, our proposed adaptation-aware FSIG method can

TABLE 2: FSIG (10-shot) results: We report FID scores (\downarrow) of AdAM (ours) and compare with existing methods for FSIG. We emphasize that Cat, Dog, and Wild target domains are additional experiments included in this work (Sec 3.1). Our experiment results show two important findings: **1)** Under setups where the assumption of close proximity between source and target domains is relaxed (Cat, Dog, Wild), SOTA FSIG methods – EWC, CDC, DCL, RSSA, LLN – which consider only the source domain in knowledge preserving perform *no better* than a baseline fine-tuning method (TGAN). **2)** Our proposed adaptation-aware AdAM achieves SOTA performance in all target domains due to preserving source domain knowledge that is important for few-shot target domain adaptation. We generate 5,000 images using the adapted generator to evaluate FID on the whole target domain. Additional results (e.g., KID) are in the Supplement.

Method	Babies [4]	Sunglasses [4]	MetFaces [39]	Sketches [61]	AFHQ-Cat [5]	AFHQ-Dog [5]	AFHQ-Wild [5]
TGAN [18]	104.79 \pm 0.03	55.61 \pm 0.04	76.81 \pm 0.04	53.41 \pm 0.02	64.68 \pm 0.03	151.46 \pm 0.05	81.30 \pm 0.02
TGAN+ADA [39]	102.58 \pm 0.12	53.64 \pm 0.08	75.82 \pm 0.06	66.99 \pm 0.01	80.16 \pm 0.20	162.63 \pm 0.31	81.55 \pm 0.17
BSA [17]	140.34 \pm 0.01	76.12 \pm 0.01	93.42 \pm 0.03	69.32 \pm 0.02	154.62 \pm 0.05	158.32 \pm 0.04	168.12 \pm 0.07
FreezeD [19]	110.92 \pm 0.02	51.29 \pm 0.05	73.33 \pm 0.07	46.54 \pm 0.01	63.60 \pm 0.08	157.98 \pm 0.28	77.18 \pm 0.13
MineGAN [62]	98.23 \pm 0.03	68.91 \pm 0.03	81.70 \pm 0.07	64.34 \pm 0.02	70.98 \pm 0.04	148.51 \pm 0.03	59.53 \pm 0.05
EWC [20]	87.41 \pm 0.02	59.73 \pm 0.04	62.67 \pm 0.09	71.25 \pm 0.01	74.61 \pm 0.17	158.78 \pm 0.14	92.83 \pm 0.15
CDC [16]	74.39 \pm 0.03	42.13 \pm 0.04	65.45 \pm 0.08	45.67 \pm 0.02	176.21 \pm 0.09	170.95 \pm 0.11	135.13 \pm 0.10
DCL [21]	52.56 \pm 0.02	38.01 \pm 0.01	62.35 \pm 0.07	37.90 \pm 0.02	156.82 \pm 0.04	171.42 \pm 0.14	115.93 \pm 0.09
RSSA [22]	75.67 \pm 0.39	44.35 \pm 0.06	57.06 \pm 0.07	54.58 \pm 0.51	166.89 \pm 0.06	158.20 \pm 0.34	162.80 \pm 0.48
LLN [23]	63.31 \pm 0.05	35.64 \pm 0.15	87.21 \pm 0.05	35.59\pm0.13	209.95 \pm 0.12	216.31 \pm 0.77	254.89 \pm 0.31
AdAM (Ours)	48.83\pm0.03	28.03\pm0.07	51.34\pm0.06	36.44\pm0.29	58.07\pm0.13	100.91\pm1.01	36.87\pm0.23

generate substantially high-quality images with high diversity for both the Babies and Cat domains. We also include FID (\downarrow) [56] and Intra-LPIPS (\uparrow) [16] (for measuring diversity) in Figure 5 to quantitatively show that our proposed method outperforms existing SOTA FSIG methods [16], [20], [21], [22], [23].

5.3 Quantitative Results

We show complete FID (\downarrow) scores (with standard deviation computed by running three times) in Table 2. Our proposed AdAM for FSIG achieves SOTA results across all target domains of varying proximity to the source (FFHQ). We emphasize that it is achieved by preserving source domain knowledge that is important for target domain adaptation (Sec. 4). We also report Intra-LPIPS (\uparrow) as an indicator of diversity, as Figure 5.

We remark that the goal of importance probing (denoted as “IP”) is to identify kernels that are important for *few-shot target adaptation* as shown in Figure 6 (Top). To justify the effectiveness of our design choice, we perform an ablation study that discards the IP stage and regards all kernels as *equally important* for target adaptation. Therefore, we simply modulate all kernels *without any knowledge selection*. As one can observe from Figure 6 (Bottom), knowledge selection plays a vital role in adaptation performance. Specifically, the significance of knowledge preservation is more evident when the target domains are distant from the source domain.

6 ANALYSIS AND ABLATION STUDIES

6.1 Effectiveness of Importance Probing

In this section, we conduct extensive and comprehensive ablation studies to show the significance of our proposed method for FSIG. Similar to the main experiments in Sec. 5, we use FFHQ [3] as the source domain, and use Babies and Cat [5] as target domains. The different approaches in this study are as follows:

TGAN [18]: The source GAN models pretrained on FFHQ are updated using *simple fine-tuning* of all parameters with the 10-shot target samples.

EWC [20]: Following [20], an L2 regularization is applied to all model weights to augment simple fine-tuning. The regularization is scaled by the importance of individual model weights as determined by the FI of the model weights based on the *source* models.

EWC + IP: We apply our probing idea on top of EWC. In the probing step, original EWC as discussed above is used but with a small number of iterations. At the end of probing, the FI of model weights based on the *updated* models is computed. Then, during main adaptation, this *target-aware* FI is used to scale the L2 regularization. In other words, EWC + IP is a target-aware version of EWC in [20] using our probing idea.

AdaFM [44]: AdaFM (see Sec. 2) is applied to all kernels.

AdaFM + IP: We apply our probing idea on top of AdaFM. In the probing step, the original AdaFM as discussed above is used but with a small number of iterations. At the end of probing, the FI of AdaFM parameters is computed, and kernels are classified as important/unimportant using the same quantile threshold $t_h\%$ as in our work. Then, during the main adaptation, the important kernels are updated via AdaFM, and the unimportant kernels are updated via simple fine-tuning. In other words, AdaFM + IP is a target-aware version of AdaFM using our probing idea.

Ours w/o IP (i.e. main adaptation only): KML modulation is applied to all kernels.

Ours w/ Freeze: We apply our probing idea as discussed in Sec. 4, i.e., with KML applied to all kernels but adaptation with a small number of iterations. At the end of probing, FI of KML parameters is computed, and kernels are classified as important/unimportant using the same quantile threshold $t_h\%$ as in our work. Then, during the main adaptation, the important kernels are *frozen*, and the unimportant kernels are updated via simple fine-tuning. In other words, this is similar to our proposed method except that kernel freezing is used in the main adaptation instead of KML for important kernels.

Ours w/ KML (i.e. AdAM): We apply our probing idea as discussed in Sec. 4, i.e., with KML applied to all kernels but adaptation with a small number of iterations. At the end of probing, FI of KML parameters is computed, and kernels are classified as important/unimportant using quantile threshold $t_h\%$ (to be discussed in Sec. 6.2). Then, during the main adaptation, the important kernels are modulated by KML, and the unimportant kernels are updated via simple fine-tuning.

Qualitative Results. We show generated images corresponding to approaches discussed above in Figure 7. These results show that our proposed idea on importance probing is principally a suitable approach to improve FSIG by identifying kernels important for

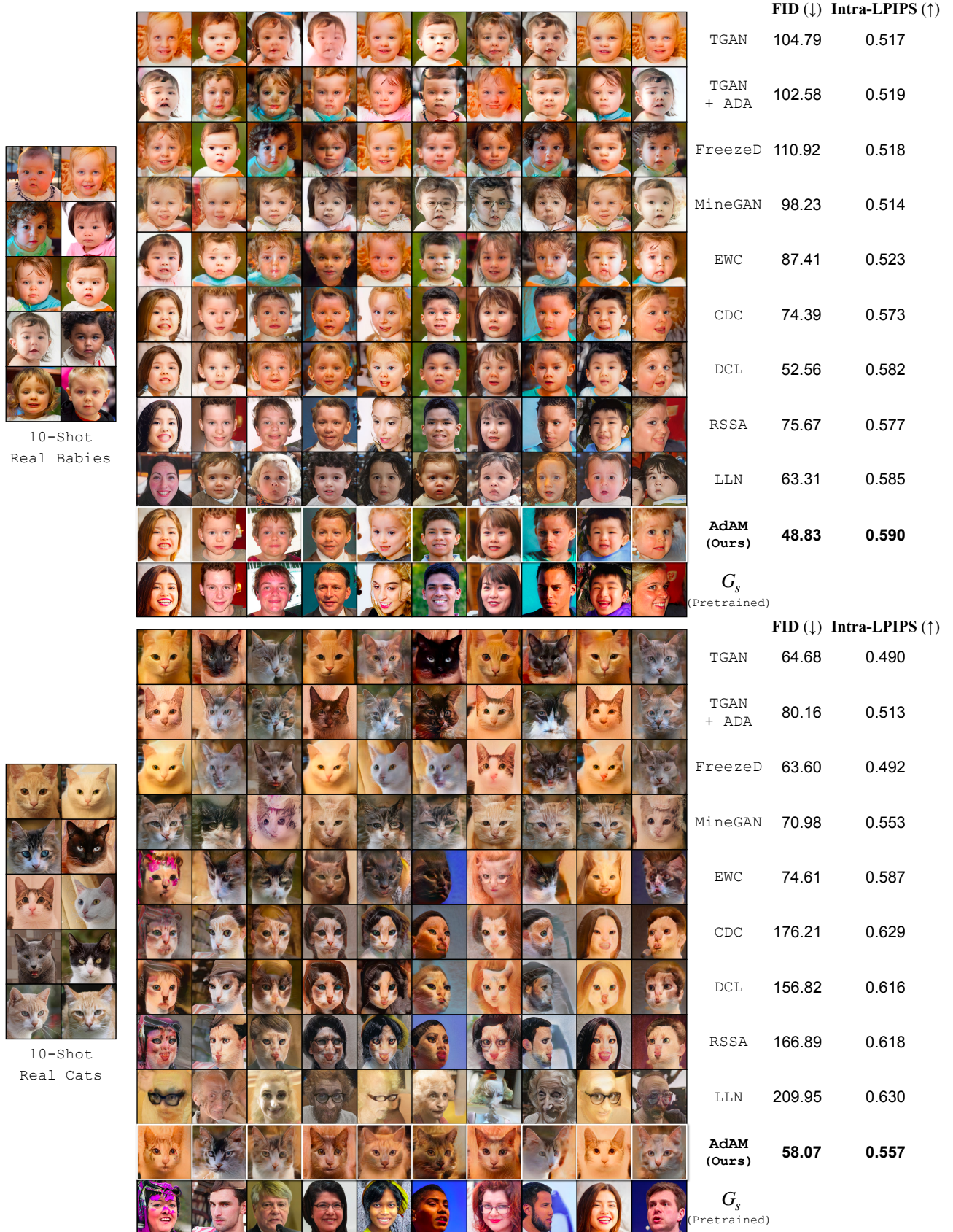


Fig. 5: Qualitative and quantitative comparison of 10-shot image generation with different FSIG methods. Images of each column are from the same noise input (except for LLN [23] where the images are randomly sampled, due to LLN directly learns a latent code in \mathcal{W}^+ space). For target domains with close proximity (e.g. Babies, **top**), our method can generate high-quality images with more refined details and diversity knowledge, achieving the best FID and Intra-LPIPS score. For target domain that is distant (e.g., Cat, **bottom**), TGAN/FreezeD overfit to the 10-shot samples and others fail. In contrast, our method preserves meaningful semantic features at different levels (e.g., posture and color) from the source, achieving a good trade-off between quality and diversity of the generated images.

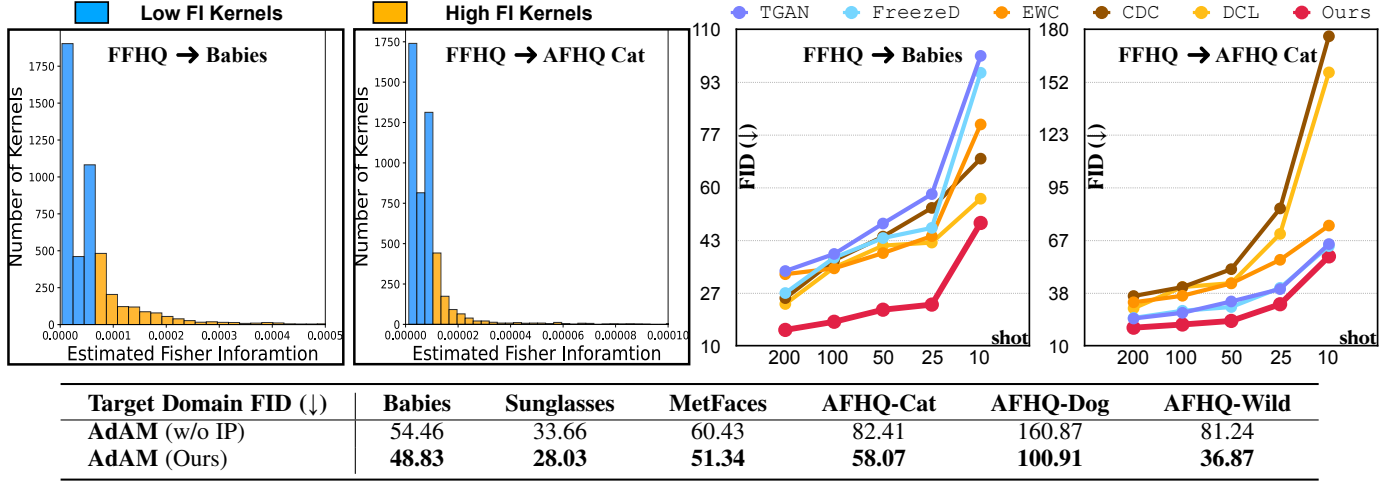


Fig. 6: **(Top Left)** Our proposed IP (in AdAM) identifies and preserves source kernels important (high FI) for target adaptation. **(Bottom)** FID score on different datasets. We validate the effectiveness of IP by modulating all kernels without IP. On the other hand, if we fine-tune all parameters without IP and modulation (TGAN), it suffers mode collapse (Table 2 and Figure 5). **(Top Right)** We evaluate the performance with different number of shots (10, 25, 50, 100, 200) on Babies and AFHQ-Cat. We show that our method consistently outperforms other FSIG methods in all setups. The complete comparison is in Table 4. In our Supplement, we also show the comparison of generated images given more target domain images (e.g. 100-shot) during adaptation.

TABLE 3: Quantitative results for IP: For each method, best FID and LPIPS results are shown in **bold**. IP is performed for 500 iterations (where relevant). These results show that our proposed IP is principally a suitable approach for FSIG. This can be clearly observed when applying IP to EWC [20] (EWC+IP) and AdaFM [44] (AdaFM+IP). We also observe that methods performing IP at kernel level (Ours w/ KML, AdaFM + IP) perform better than method performing IP at parameter level (EWC + IP). Overall, we quantitatively show that our proposed method outperforms all existing FSIG methods with IP, thereby generating images with high quality (FID \downarrow) and good diversity (Intra-LPIPS \uparrow).

Method	FFHQ \rightarrow Babies		FFHQ \rightarrow Cat	
	FID (\downarrow)	Intra-LPIPS (\uparrow)	FID (\downarrow)	Intra-LPIPS (\uparrow)
TGAN [18]	104.79	0.517	64.68	0.490
EWC [20]	87.41	0.521	74.61	0.587
EWC + [IP (Ours)]	70.80	0.625	66.35	0.540
AdaFM [44]	62.90	0.568	64.44	0.525
AdaFM + [IP (Ours)]	55.64	0.577	60.04	0.540
Ours w/o IP	54.46	0.613	82.41	0.522
Ours w/ Freeze [w/ IP]	50.81	0.581	61.60	0.559
AdAM (w/ KML [w/ IP])	48.83	0.590	58.07	0.557

target domain adaptation. Figure 7 also shows that our proposed method can generate images with better quality.

Quantitative results. We show FID (\downarrow) / LPIPS (\uparrow) results in Table 3, which demonstrates our proposed IP is principally a suitable approach for FSIG. This can be clearly observed when applying IP to EWC [20] and AdaFM [44]. We remark that probing with KML (AdAM) is computationally more efficient compared to probing with EWC and AdaFM due to less trainable parameters (see Supplement). Overall, we show that our proposed method outperforms existing FSIG methods with IP, thereby generating images with a good balance between quality (FID \downarrow) and diversity (Intra-LPIPS \uparrow). We also empirically observe that methods performing IP at kernel level (AdAM, AdaFM + IP) perform better than methods performing IP at parameter level (EWC + IP).

6.2 Threshold of Preserving Important Kernels

Our proposed AdAM for FSIG aims to preserve different amount of source knowledge that is useful for target adaptation. Specifically, we preserve filters that are deemed important for target adaptation by modulating them via parameter-efficient KML (see Figure 4). We select the high-importance filters by using a quantile $t_h(\%)$ as a threshold to determine the importance of a kernel. In this section, we conduct a study to show the effectiveness and impact of preserving different amount of filters that are deemed to be most relevant for target adaptation.

As shown in Figure 8, varying the amount of filters for preservation improves the performance in different ways. In practice, we select $t_h=50\%$ for FFHQ \rightarrow Babies and $t_h=75\%$ for FFHQ \rightarrow AFHQ-Cat, and this choice is also intuitive: for target domains that are semantically closer to the source, preserving more source knowledge might be useful for few-shot adaptation.

6.3 Number of Target Samples (shots)

The number of target domain training samples is an important factor that can impact the FSIG performance. In general, more target domain samples can allow better estimation of the target distribution. We empirically study the efficacy of our proposed method under different number of target domain samples. A direct comparison is shown in Figure 6 and the complete quantitative results are in Table 4. We show that our proposed adaptation-aware FSIG method consistently outperforms existing SOTA methods in different source \rightarrow target setups with different proximity, even when adapting the model to the entire target domain samples.

6.4 Alternative Importance Measure

In literature, Class Saliency [63] (CS) is used as a property to explain which area/pixels of an input image stand out for a specific classification decision. Similar to the estimated Fisher Information (FI) used in our work, the complexity of CS is based on the first-order derivatives. Therefore, conceptually CS could have a

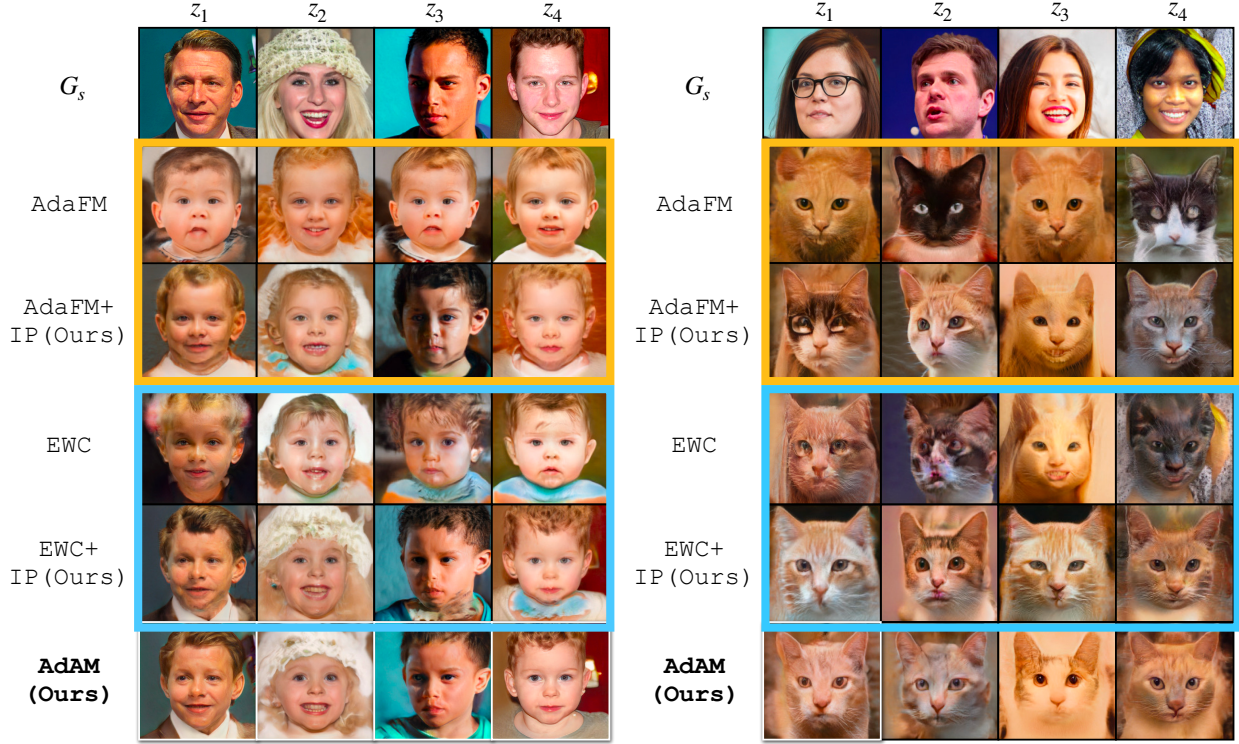


Fig. 7: **Qualitative results of the effectiveness of Importance Probing (IP).** G_s is the source generator (FFHQ). We show results for our major setups, FFHQ \rightarrow Babies (left) and FFHQ \rightarrow Cat (right). Applying IP to EWC [20], AdaFM [44], we observe better quality in FSIG. This shows that our proposed idea probing the importance of kernels for FSIG is principally a suitable approach to improve FSIG on various methods. One can also observe that images generated by our proposed method with KML, e.g. the last row, has good quality compared to other methods. Our observation is quantitatively confirmed in Table 3 .

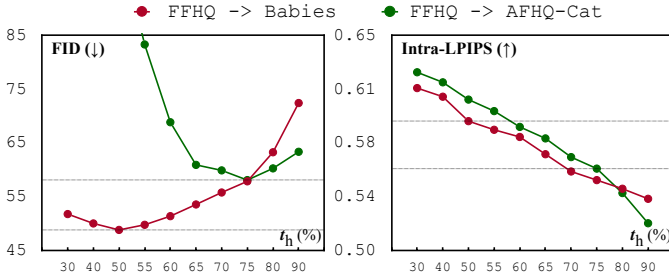


Fig. 8: Evaluation of the performance by varying the thresholds for preserving important kernels. In practice, we choose $t_h=50\%$ for close target domains (e.g., Babies) and $t_h=75\%$ for remote target domains (e.g., Cats) which empirically obtain the best performance.

connection with FI as they both use the knowledge encoded in the gradients.

We perform an experiment to replace FI with CS in importance probing and compare it with our original approach. Note that, in [63], CS is computed w.r.t. input image pixels. To make CS suitable for our problem, we modify it and compute CS w.r.t. modulation parameters. Similar to our approach in Sec. 4, we average the importance of all parameters within a kernel to calculate the importance of that kernel. Then we use these values during our importance probing to determine the important kernels for adapting from source to target domain (as Sec. 4). The results in Table 5 are obtained with our proposed method using FI and CS during importance probing.

Our results suggest that importance probing using FI (approx-

mated by first-order derivatives) can perform better in the selection of important kernels, leading to better performance (FID, intra-LPIPS) in the adapted models as shown in Table 5.

6.5 Discussion: How much can the proximity between source and target domain be relaxed?

In this section, we discuss the proximity limitation between source domain \mathcal{S} and target domain \mathcal{T} in our experiment setups. First, we remark that the upper bound on proximity between \mathcal{S} and \mathcal{T} could be conditioning on (a): the number of available samples (shots) from the target domain, and (b): the method used for knowledge transfer.

(a): Proximity bound conditioning on the number of target domain samples. In this paper, we focus on few-shot setups, e.g. 10 shots. However, with more target domain samples available, proximity between \mathcal{S} and \mathcal{T} can be further relaxed, and the proximity bound would increase, i.e. for a given generative model on \mathcal{S} , we could learn an adapted model for \mathcal{T} which is more distant. Intuitively, increasing the number of target domain samples can provide more diverse knowledge for \mathcal{T} , and as a result, there is less reliance on the knowledge of \mathcal{S} that is generalizable for \mathcal{T} (which would decrease as \mathcal{S} and \mathcal{T} are more apart). In the limiting cases when abundant target domain samples are available, knowledge of \mathcal{S} would not be critical, and proximity constraints between \mathcal{S} and \mathcal{T} may be totally relaxed (ignored).

(b): Proximity bound conditioning on the knowledge transfer method. Given a generative model pretrained on \mathcal{S} and a certain number of available samples from \mathcal{T} , the method used for knowledge transfer plays a critical role. If the method is superior

TABLE 4: We conduct comprehensive experiments to evaluate the performance, i.e., FID (\downarrow) of different few-shot generation methods, given different number of shots for adaptation: from one-shot to the entire dataset. The images for adaptation are randomly sampled and kept the same for all methods for fair comparison. The results are as below. **Top:** FFHQ \rightarrow Babies. **Bottom:** FFHQ \rightarrow Cat.

Number of Shots	TGAN	TGAN+ADA	EWC	CDC	AdAM
1	172.49	188.84	104.50	88.86	77.71
5	108.65	105.19	88.51	78.29	52.85
10	104.79	102.58	87.41	74.39	48.83
25	57.94	58.86	44.67	53.58	23.05
50	48.65	52.18	39.32	44.52	21.44
100	39.04	45.71	34.49	37.04	17.63
200	33.65	38.84	32.65	25.1	15.06
500	27.21	26.31	28.11	22.53	14.71
1000	25.68	25.30	25.55	21.79	14.12
All Samples (~ 2700)	25.03	25.47	24.57	21.91	13.59

Number of Shots	TGAN	TGAN+ADA	EWC	CDC	AdAM
1	125.52	125.81	139.11	197.79	118.25
5	90.24	86.94	136.65	180.34	79.53
10	64.68	80.16	74.61	176.21	58.07
25	40.52	48.61	56.23	83.80	32.38
50	33.87	35.76	43.58	51.20	26.43
100	27.78	28.16	36.93	41.58	21.50
200	24.73	26.78	33.43	36.79	19.79
500	20.25	19.01	32.73	30.81	14.80
1000	17.20	16.46	31.50	28.50	16.80
All Samples (~ 5000)	10.52	9.56	18.76	20.53	6.52

TABLE 5: **Additional Importance Measure.** In this experiment, we replace Fisher Information (FI) with Class Saliency (CS) [63] in importance probing and compare with our original approach. We evaluate the performance under different source \rightarrow target adaptation setups.

Importance Measure	FFHQ \rightarrow Babies		FFHQ \rightarrow Cat	
	FID (\downarrow)	Intra-LPIPS (\uparrow)	FID (\downarrow)	Intra-LPIPS (\uparrow)
Class Saliency [63]	52.46	0.582	61.68	0.556
Fisher Information (Ours)	48.83	0.590	58.07	0.557

in identifying suitable transferable knowledge from \mathcal{S} to \mathcal{T} , the proximity between \mathcal{S} and \mathcal{T} can be relaxed, and the proximity bound would increase. In our work, our first contribution is to reveal that existing SOTA approaches (which are based on target-agnostic ideas) are inadequate in identifying transferable knowledge from \mathcal{S} to \mathcal{T} . As a result, when proximity between \mathcal{S} and \mathcal{T} is relaxed, the performance of the adapted models is miserably poor, as discussed in Sec. 3, Sec. 5 and Supplement. Therefore, our second contribution is to propose a target-aware approach that could identify more meaningful transferable knowledge from \mathcal{S} to \mathcal{T} , allowing relaxation of the proximity constraint.

In this section, we provide experimental results for the adaptation between two very distant domains: FFHQ \rightarrow Cars using only 10 shots, aiming to answer two main questions: (1) Is there transferable knowledge from FFHQ to Cars for the FSIG task? (2) How does AdAM (our) compare with other methods in this setup? For this, in addition to transfer learning approaches discussed in the paper, we also add the results for training from scratch using only the same 10 Car samples. The results are in Table 6.

6.6 Additional Source \rightarrow Target Results

In this section, we show additional 10-shot adaptation results for our proposed adaptation-aware FSIG method for target domains

TABLE 6: We conduct experiments for FFHQ (\mathcal{S}) \rightarrow Cars (Remote domain \mathcal{T}) adaptation and evaluate the performance in such a challenging setup. We show that our method can achieve similar diversity as ADA [39] and the overall performance (FID) is better than other baseline and SOTA methods.

Method	FFHQ \rightarrow Cars (Remote domain)	
	FID (\downarrow)	Intra-LPIPS (\uparrow)
Training from Scratch	201.34	0.300
TGAN+ADA [39]	171.98	0.438
EWC [20]	276.19	0.620
CDC [16]	109.53	0.484
DCL [21]	125.96	0.464
AdAM (Ours)	80.55	0.425

TABLE 7: Performance with additional GAN architecture. In this experiment, we use ProGAN [64] as the GAN model and compare with other baseline and SOTA methods. We evaluate the performance under different source \rightarrow target adaptation setups.

Method	FFHQ \rightarrow Babies		FFHQ \rightarrow Cat	
	FID (\downarrow)	Intra-LPIPS (\uparrow)	FID (\downarrow)	Intra-LPIPS (\uparrow)
TGAN [18]	86.91	0.507	78.89	0.522
TGAN + ADA [39]	83.09	0.555	89.53	0.559
EWC [20]	80.77	0.559	151.39	0.593
AdAM (Ours)	75.77	0.567	72.85	0.546

with different proximity. Visualization and comparison results are shown in Figure 9 and in our Supplement. As one can observe, SOTA FSIG methods [16], [20], [21] are unable to adapt well to distant target domains due to only considering source task in knowledge preservation, while TGAN [18] suffers severe mode collapse. In contrast, AdAM (our) outperforms these methods and consistently produces high quality images with good diversity.

6.7 Additional GAN Architectures

We use an additional pre-trained GAN architecture, ProGAN [64], to conduct FSIG experiments for FFHQ \rightarrow Babies, FFHQ \rightarrow Cat, Church \rightarrow Haunted houses and Church \rightarrow Palace setups. For fair comparison, we strictly follow the exact experiment setup discussed in Sec. 5.

Results. We show qualitative and quantitative results for FFHQ \rightarrow Babies, FFHQ \rightarrow Cat adaptation in Figure 10 and Table 7. As one can observe, our proposed method consistently outperforms other baseline and SOTA FSIG methods with another pre-trained GAN model (ProGAN [64]), demonstrating the effectiveness and generalizability of our method. We also show qualitative results and analysis for Church \rightarrow Haunted houses and Church \rightarrow Palace adaptation in Supplement.

7 EXPLAINABLE ADAM FOR EFFECTIVE KNOWLEDGE TRANSFER

In this section, we attempt to discover what form of visual information is encoded/generated by a specific high FI kernel identified by our importance probing algorithm in AdAM, and how it is preserved after target adaptation in FSIG.

7.1 What form of visual information is encoded by high FI kernels in AdAM?

This is a natural and complex problem and to our best knowledge, methods on visualizing generative models/GANs are still rather

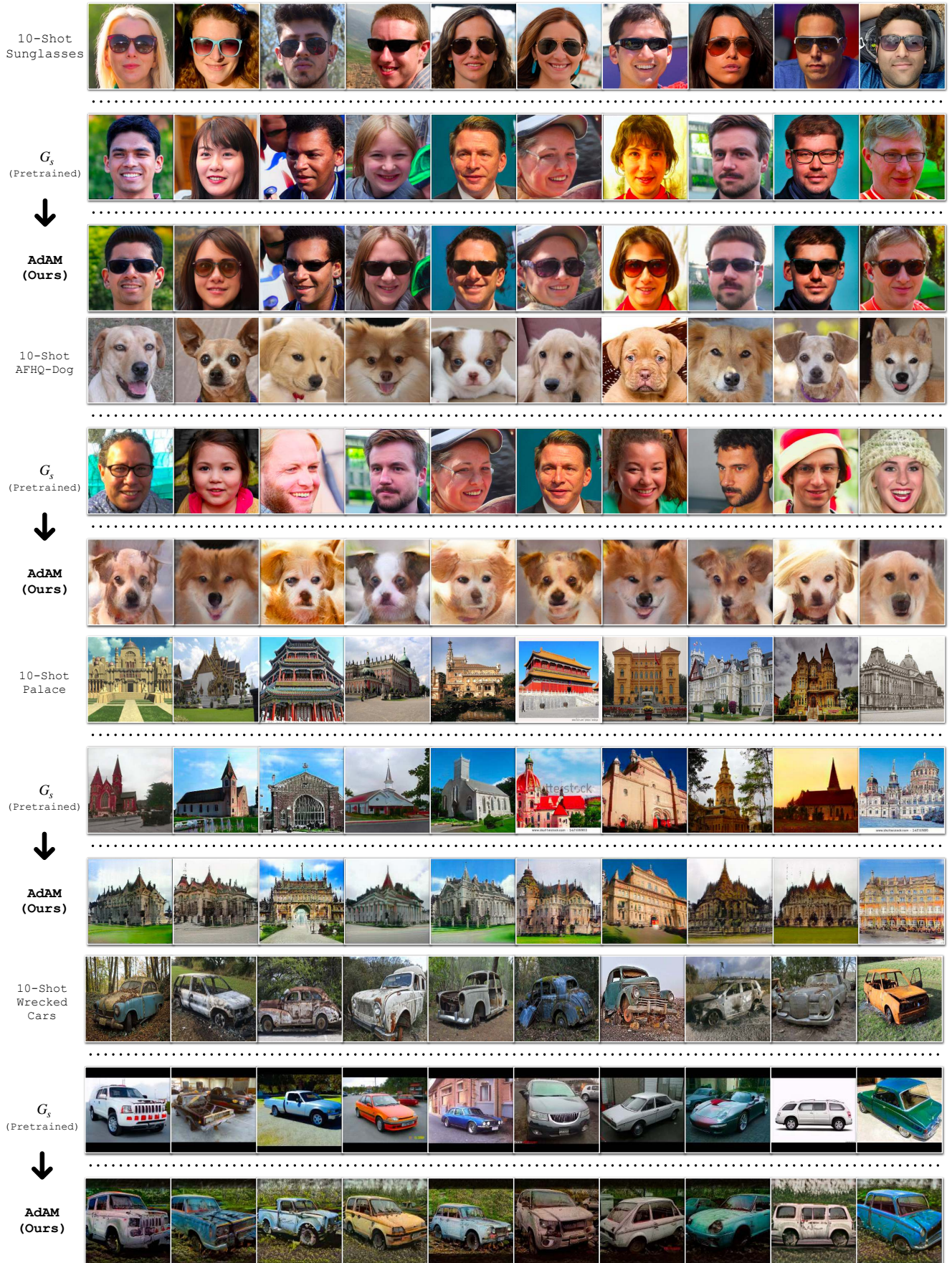


Fig. 9: Few-shot adaptation results. We show that AdAM can adapt the source GAN to target domains with different proximity to the source given only few-shot samples. 1. FFHQ \rightarrow Sunglasses. 2. FFHQ \rightarrow AFHQ-Dog. 3. LSUN Church \rightarrow Palace. 4. LSUN Cars \rightarrow Wrecked Cars. Additional adaptation results with more source/target domains are in our Supplement.

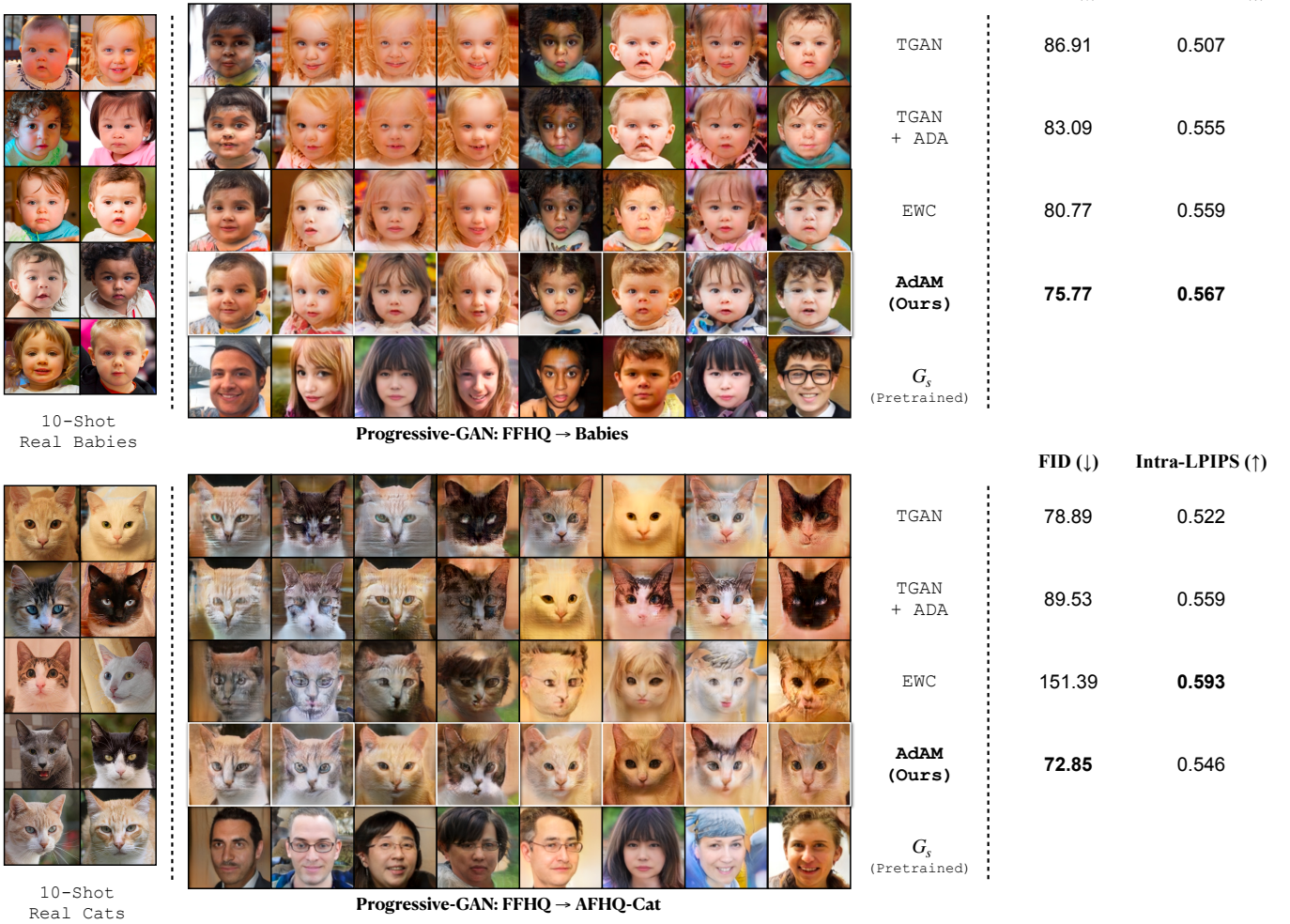


Fig. 10: Qualitative and quantitative 10-shot adaptation results of FFHQ → Babies and FFHQ → Cat using pre-trained ProGAN [64]. As one can observe, our proposed method outperforms existing FSIG methods. More results are in the Supplement.

restrictive in terms of concepts or knowledge that can be visualized. Nevertheless, we leverage on GAN Dissection [57], a more established visualization method and explainable tool to visualize the internal representations that are highly correlated to important (high FI) kernels identified by our probing algorithm.

Experiment setup: We use LSUN-Church as the source domain, this is because the official GAN Dissection method [65] is more suitable for *scene-based* image generators (and due to the limitation of the semantic segmentation used in the GAN Dissection pipeline [57]). We use the Palace from ImageNet-1K as the target domain. Following official GAN Dissection implementation [57], we use the ProGAN [64] model. For fair comparison, we strictly follow the exact experiment setup discussed in Sec. 5 and Sec. 6.

Results: Visualizing high FI kernels for Church → Palace adaptation: The results for importance estimation (via FI) for kernels and several distinct semantic concepts learnt by high FI kernels are shown in Figure 11. We visualize four examples of high FI kernels: (a), (b), (c), (d) corresponding to concepts building, dome, window and sky/cloud, respectively. Using GAN Dissection, we observe that a notable amount of high FI kernels correspond to useful source domain concepts which are preserved when adapting to Palace target domain. We remark that these preserved concepts encoded by high FI kernels (and determined by AdAM) are useful

to the target domain adaptation (See the bottom side of Figure 11).

Transferability of high FI kernels for FSIG: We remark that, the distinct semantic concepts (examples in Figure 11) encoded by the high FI kernels, and identified / preserved by AdAM, are effectively transferred to the target domain after few-shot adaptation, leading to the high quality and diversity of generated images of the resulting target generator. We further note that our observation is consistent with different GAN architectures and various source → target adaptation setups, e.g., StyleGAN-V2 in Figure 7, Figure 9, and ProGAN results in Figure 10. Additional results are included in our Supplement.

7.2 Limitations and Future Work of GAN Dissection

In our experiments, although GAN Dissection can uncover useful semantic concepts and knowledge preserved by high FI kernels, GAN Dissection method [57] is limited by the datasets and models used for semantic segmentation. Hence this method is not able to uncover concepts that are not present in semantic segmentation dataset (They use Broaden Dataset [58]). Therefore, using GAN dissection we are currently unable to discover and visualize more fine-grained concepts preserved by our high FI kernels. On the other hand, the GAN dissection method [57] is built on top of ProGAN image generators, and it is still challenging to dissect

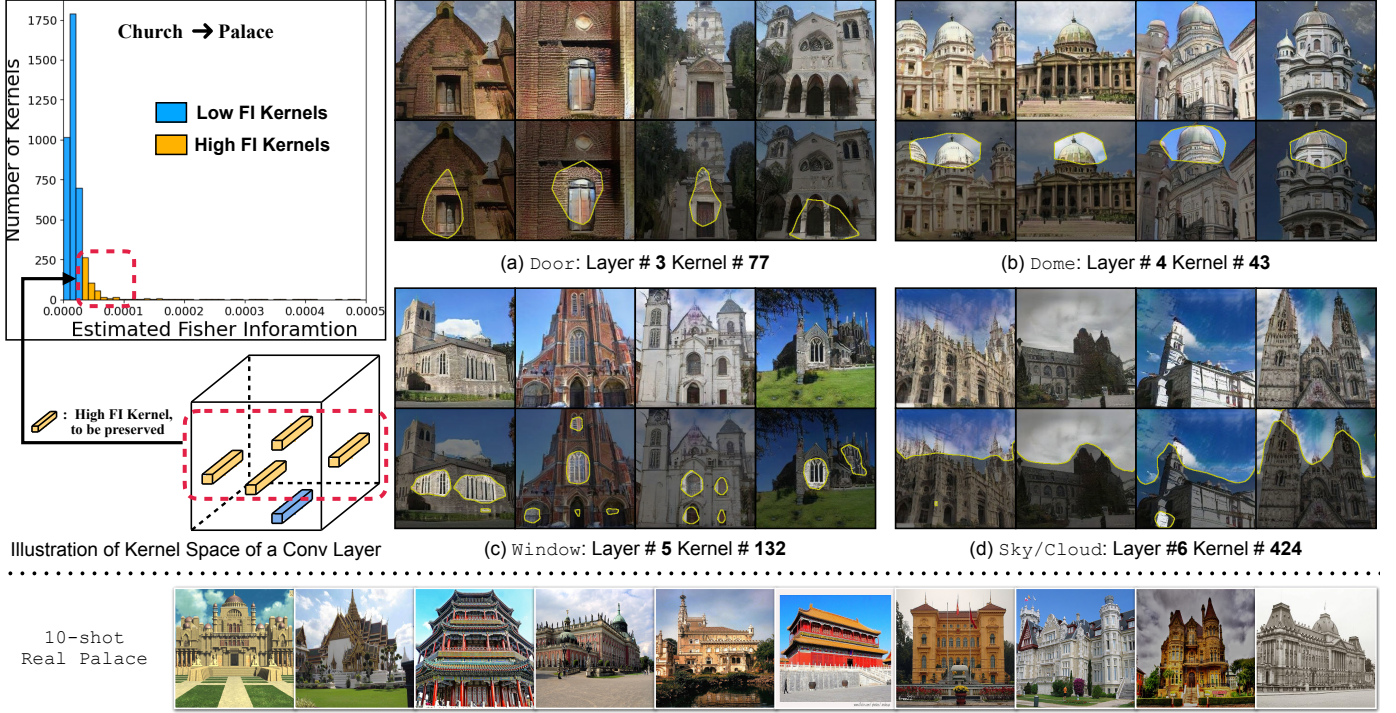


Fig. 11: **Top:** Visualizing high FI kernels using GAN Dissection [57] for Church \rightarrow Palace 10-shot adaptation. (Left) Illustration of kernel space of a Conv layer in the source generator and the estimated FI of source kernels for the target (Palace) FSIG adaptation. (Right) The visualization of different high FI kernels and the corresponding distinct semantics. The first row shows different images generated by the source generator, and the second row highlights the concept encoded by the corresponding high FI kernel as determined by GAN Dissection. We observe that a notable amount of high FI kernels correspond to useful source domain concepts including (a) building, (b) dome, (c) window, and (d) sky/cloud, which are preserved when adapting to the target domain (Palace in this figure). **Bottom:** 10-shot real Palace images as target samples. **Importantly**, we remark that the concepts encoded by high FI kernels determined by AdAM are useful and transferrable to the target domain adaptation. Best viewed in color with zooming in.

image generators with more complex and advanced structures. Nevertheless, we remark that we have consistent observation on dissection/transferrability results that demonstrate the effectiveness of our proposed AdAM for FSIG tasks.

8 DISCUSSION

8.1 Conclusions

Focusing on FSIG, we make two contributions. First, we revisit current SOTA methods and their experiments. We discover that SOTA methods perform poorly in setups when source and target domains are more distant, as existing methods only consider source domain/task for knowledge preservation. Second, we propose a new FSIG method which is target/adaptation-aware (AdAM). Our proposed method outperforms previous work across all setups of different source-target domain proximity. We include rich extended experiments and analysis in the Supplement.

8.2 Limitations and Future Works

While our experiments are extensive compared to previous works, in practical applications, there are many possible target domains which cannot be included in our experiments. However, as our method is target/adaptation aware, we believe our method can generalize better than existing SOTA which are target-agnostic.

8.3 Broader Impact

Our work makes contribution to the generation of synthetic data in applications where sample collection is challenging, e.g., photos of rare animal species. This is an important contribution to many data-centric applications. Furthermore, transfer learning of generative models using a few data samples enables data and computation-efficient model development and has positive impact on environmental sustainability and the reduction of greenhouse gas emissions. While our work targets generative applications with limited data, it parallelly raises concerns regarding such methods being used for malicious purposes. Given the recent success of forensic detectors [68], [69], [70], [71], [72], we conduct a simple study using Color-Robust forensic detector proposed in [68] on our Babies and Cat datasets. We observe that the model achieves 99.8% and 99.9% average precision (AP) respectively showing that AdAM samples can be successfully detected. We also remark that our work presents opportunities for improving knowledge transfer methods [32], [73], [74], [75], [76] in a broader context.

8.4 Potential Risks and Ethical Concerns

Given very limited target domain samples (e.g., 10-shot), our proposed method for FSIG is lightweight and achieves state-of-the-art results with different source/target domain proximity. Though our work shows exciting results by pushing the limits of FSIG, we urge researchers, practitioners, and developers to use our work with privacy, ethical and moral concerns. In what next, we bring an example to our discussion.



Fig. 12: FFHQ \rightarrow Obama photo (from Obama Dataset [66]). We demonstrate that, given very few photo(s), our algorithm can generate diverse images of a particular person, similar to some recent popular models, e.g., DreamBooth [67]. Consequently, we urge researchers and practitioners to attend to safety and ethical concerns before using/deploying our method. More details in Sec. 8.4.

Adapting our algorithm to a particular person. The idea of FSIG aims to adapt a pretrained GAN to a target domain with limited samples. Consequently, it is possible and reasonable that a user of FSIG can take few-shot images of a particular person and generate diverse images of the person, which leads to potential safety and privacy concerns. We conduct an experiment to adapt a pretrained StyleGAN-V2 generator to a single Obama photo [66]. The visualization results and analysis are shown in Figure 12. On the other hand, our method can be adapted to generate images of the same person by applying a more restrictive selection of the source model’s knowledge. However, this would degrade the diversity of the outputs and may not be suitable for general FSIG which our paper focuses on.

Our model is lightweight for deployment. Compared to some recent multi-modal text-to-image generative models, e.g., Stable Diffusion [77] for few-shot adaptation tasks, e.g., DreamBooth [67] and Textual Inversion [78], our proposed method for GAN-based few-shot image generation can be easily applied on edge devices, due to the lightweight model size (Stable Diffusion has ~ 890 M parameters and StyleGAN-V2 generator has around ~ 30 M parameters, which is ~ 30 times less scale). Therefore, it is vital for users of our algorithms to bear in mind these ethical concerns.

REFERENCES

- [1] I. Goodfellow, J. Pouget-Abadie, M. Mirza, B. Xu, D. Warde-Farley, S. Ozair, A. Courville, and Y. Bengio, “Generative adversarial nets,” *Advances in neural information processing systems*, vol. 27, 2014.
- [2] A. Brock, J. Donahue, and K. Simonyan, “Large scale gan training for high fidelity natural image synthesis,” *International Conference on Learning Representations*, 2018.
- [3] T. Karras, S. Laine, M. Aittala, J. Hellsten, J. Lehtinen, and T. Aila, “Analyzing and improving the image quality of stylegan,” in *Proceedings of the IEEE/CVF Conference on Computer Vision and Pattern Recognition*, 2020, pp. 8110–8119.
- [4] T. Karras, S. Laine, and T. Aila, “A style-based generator architecture for generative adversarial networks,” in *Proceedings of the IEEE/CVF conference on computer vision and pattern recognition*, 2019, pp. 4401–4410.
- [5] Y. Choi, Y. Uh, J. Yoo, and J.-W. Ha, “Stargan v2: Diverse image synthesis for multiple domains,” in *Proceedings of the IEEE Conference on Computer Vision and Pattern Recognition*, 2020.
- [6] J.-Y. Zhu, T. Park, P. Isola, and A. A. Efros, “Unpaired image-to-image translation using cycle-consistent adversarial networks,” in *Proceedings of the IEEE international conference on computer vision*, 2017, pp. 2223–2232.
- [7] M.-Y. Liu, X. Huang, A. Mallya, T. Karras, T. Aila, J. Lehtinen, and J. Kautz, “Few-shot unsupervised image-to-image translation,” in *Proceedings of the IEEE/CVF International Conference on Computer Vision*, 2019, pp. 10551–10560.
- [8] J. Lin, R. Zhang, F. Ganz, S. Han, and J.-Y. Zhu, “Anycost gans for interactive image synthesis and editing,” in *Proceedings of the IEEE/CVF Conference on Computer Vision and Pattern Recognition*, 2021, pp. 14986–14996.
- [9] H. Liu, Z. Wan, W. Huang, Y. Song, X. Han, J. Liao, B. Jiang, and W. Liu, “Deflocnet: Deep image editing via flexible low-level controls,” in *Proceedings of the IEEE/CVF Conference on Computer Vision and Pattern Recognition*, 2021, pp. 10765–10774.
- [10] S. K. Lim, Y. Loo, N. T. Tran, N. M. Cheung, G. Roig, and Y. Elovici, “Doping: Generative data augmentation for unsupervised anomaly detection with gan,” in *18th IEEE International Conference on Data Mining, ICDM 2018*. Institute of Electrical and Electronics Engineers Inc., 2018, pp. 1122–1127.
- [11] N.-T. Tran, V.-H. Tran, N.-B. Nguyen, T.-K. Nguyen, and N.-M. Cheung, “On data augmentation for gan training,” *IEEE Transactions on Image Processing*, vol. 30, pp. 1882–1897, 2021.
- [12] L. Chai, J.-Y. Zhu, E. Shechtman, P. Isola, and R. Zhang, “Ensembling with deep generative views,” in *CVPR*, 2021.
- [13] J. Deng, W. Dong, R. Socher, L.-J. Li, K. Li, and L. Fei-Fei, “Imagenet: A large-scale hierarchical image database,” in *2009 IEEE conference on computer vision and pattern recognition*, 2009, pp. 248–255.
- [14] J. Yaniv, Y. Newman, and A. Shamir, “The face of art: landmark detection and geometric style in portraits,” *ACM Transactions on graphics (TOG)*, vol. 38, no. 4, pp. 1–15, 2019.
- [15] Q. Feng, C. Guo, F. Benitez-Quiroz, and A. M. Martinez, “When do gans replicate? on the choice of dataset size,” in *Proceedings of the IEEE/CVF International Conference on Computer Vision*, 2021, pp. 6701–6710.
- [16] U. Ojha, Y. Li, J. Lu, A. A. Efros, Y. J. Lee, E. Shechtman, and R. Zhang, “Few-shot image generation via cross-domain correspondence,” in *Proceedings of the IEEE/CVF Conference on Computer Vision and Pattern Recognition*, 2021, pp. 10743–10752.
- [17] A. Noguchi and T. Harada, “Image generation from small datasets via batch statistics adaptation,” in *Proceedings of the IEEE/CVF International Conference on Computer Vision*, 2019, pp. 2750–2758.
- [18] Y. Wang, C. Wu, L. Herranz, J. van de Weijer, A. Gonzalez-Garcia, and B. Raducanu, “Transferring gans: generating images from limited data,” in *Proceedings of the European Conference on Computer Vision (ECCV)*, 2018, pp. 218–234.
- [19] S. Mo, M. Cho, and J. Shin, “Freeze the discriminator: a simple baseline for fine-tuning gans,” in *CVPR AI for Content Creation Workshop*, 2020.
- [20] Y. Li, R. Zhang, J. C. Lu, and E. Shechtman, “Few-shot image generation with elastic weight consolidation,” in *Advances in Neural Information Processing Systems*, H. Larochelle, M. Ranzato, R. Hadsell, M. F. Balcan, and H. Lin, Eds., vol. 33. Curran Associates, Inc., 2020, pp. 15885–15896. [Online]. Available: <https://proceedings.neurips.cc/paper/2020/file/b6d767d2f8ed5d21a44b0e5886680cb9-Paper.pdf>
- [21] Y. Zhao, H. Ding, H. Huang, and N.-M. Cheung, “A closer look at few-shot image generation,” in *CVPR*, 2022.
- [22] J. Xiao, L. Li, C. Wang, Z.-J. Zha, and Q. Huang, “Few shot generative model adaption via relaxed spatial structural alignment,” in *Proceedings of the IEEE/CVF Conference on Computer Vision and Pattern Recognition*, 2022, pp. 11204–11213.
- [23] A. K. Mondal, P. Tiwary, P. Singla, and A. Prathosh, “Few-shot cross-domain image generation via inference-time latent-code learning,” in *The Eleventh International Conference on Learning Representations*, 2023.
- [24] S. J. Pan and Q. Yang, “A survey on transfer learning,” *IEEE Transactions on knowledge and data engineering*, vol. 22, no. 10, pp. 1345–1359, 2009.
- [25] J. Yaniv, Y. Newman, and A. Shamir, “The face of art: landmark detection and geometric style in portraits,” *ACM Transactions on graphics (TOG)*, vol. 38, no. 4, pp. 1–15, 2019.
- [26] A. Ly, M. Marsman, J. Verhagen, R. P. Grasman, and E.-J. Wagenmakers, “A tutorial on fisher information,” *Journal of Mathematical Psychology*, vol. 80, pp. 40–55, 2017.

- [27] L. Fei-Fei, R. Fergus, and P. Perona, “One-shot learning of object categories,” *IEEE transactions on pattern analysis and machine intelligence*, vol. 28, no. 4, pp. 594–611, 2006.
- [28] J. Snell, K. Swersky, and R. Zemel, “Prototypical networks for few-shot learning,” in *Advances in neural information processing systems*, 2017, pp. 4077–4087.
- [29] Y. Guo and N.-M. Cheung, “Attentive weights generation for few shot learning via information maximization,” in *Proceedings of the IEEE/CVF Conference on Computer Vision and Pattern Recognition*, 2020, pp. 13 499–13 508.
- [30] J. Sun, S. Lapuschkin, W. Samek, Y. Zhao, N.-M. Cheung, and A. Binder, “Explanation-guided training for cross-domain few-shot classification,” in *2020 25th International Conference on Pattern Recognition (ICPR)*. IEEE, 2021, pp. 7609–7616.
- [31] M. Abdollahzadeh, T. Malekzadeh, and N.-M. M. Cheung, “Revisit multimodal meta-learning through the lens of multi-task learning,” *Advances in Neural Information Processing Systems*, vol. 35, 2021.
- [32] Y. Zhao and N.-M. Cheung, “Fs-ban: Born-again networks for domain generalization few-shot classification,” *IEEE Transactions on Image Processing*, 2023.
- [33] W. Liu, C. Zhang, G. Lin, and F. Liu, “Crnet: Cross-reference networks for few-shot segmentation,” in *Proceedings of the IEEE/CVF Conference on Computer Vision and Pattern Recognition*, 2020, pp. 4165–4173.
- [34] M. Boudiaf, H. Kervadec, Z. I. Masud, P. Piantanida, I. Ben Ayed, and J. Dolz, “Few-shot segmentation without meta-learning: A good transductive inference is all you need?” in *Proceedings of the IEEE/CVF Conference on Computer Vision and Pattern Recognition*, 2021, pp. 13 979–13 988.
- [35] G. Zhang, K. Cui, R. Wu, S. Lu, and Y. Tian, “Pnpdet: Efficient few-shot detection without forgetting via plug-and-play sub-networks,” in *Proceedings of the IEEE/CVF Winter Conference on Applications of Computer Vision*, 2021, pp. 3823–3832.
- [36] Z. Fan, Y. Ma, Z. Li, and J. Sun, “Generalized few-shot object detection without forgetting,” in *Proceedings of the IEEE/CVF Conference on Computer Vision and Pattern Recognition*, 2021, pp. 4527–4536.
- [37] Y. Zhao, K. Chandrasegaran, M. Abdollahzadeh, and N.-M. M. Cheung, “Few-shot image generation via adaptation-aware kernel modulation,” *Advances in Neural Information Processing Systems*, vol. 35, pp. 19 427–19 440, 2022.
- [38] Y. Zhao, C. Du, M. Abdollahzadeh, T. Pang, M. Lin, S. Yan, and N.-M. Cheung, “Exploring incompatible knowledge transfer in few-shot image generation,” in *Proceedings of the IEEE/CVF Conference on Computer Vision and Pattern Recognition*, 2023, pp. 7380–7391.
- [39] T. Karras, M. Aittala, J. Hellsten, S. Laine, J. Lehtinen, and T. Aila, “Training generative adversarial networks with limited data,” *Advances in Neural Information Processing Systems*, vol. 33, pp. 12 104–12 114, 2020.
- [40] N.-T. Tran, T.-A. Bui, and N.-M. Cheung, “Dist-gan: An improved gan using distance constraints,” in *Proceedings of the European Conference on Computer Vision (ECCV)*, 2018, pp. 370–385.
- [41] H.-Y. Tseng, L. Jiang, C. Liu, M.-H. Yang, and W. Yang, “Regularizing generative adversarial networks under limited data,” in *Proceedings of the IEEE/CVF Conference on Computer Vision and Pattern Recognition*, 2021, pp. 7921–7931.
- [42] C. Zheng, B. Liu, H. Zhang, X. Xu, and S. He, “Where is my spot? few-shot image generation via latent subspace optimization,” in *Proceedings of the IEEE/CVF Conference on Computer Vision and Pattern Recognition*, 2023, pp. 3272–3281.
- [43] M. Zhao, Y. Cong, and L. Carin, “On leveraging pretrained gans for generation with limited data,” in *International Conference on Machine Learning*. PMLR, 2020, pp. 11 340–11 351.
- [44] Y. Cong, M. Zhao, J. Li, S. Wang, and L. Carin, “Gan memory with no forgetting,” *Advances in Neural Information Processing Systems*, vol. 33, pp. 16 481–16 494, 2020.
- [45] S. Varshney, V. K. Verma, P. Sriji, L. Carin, and P. Rai, “Cam-gan: Continual adaptation modules for generative adversarial networks,” *Advances in Neural Information Processing Systems*, vol. 34, 2021.
- [46] M.-E. Nilsback and A. Zisserman, “Automated flower classification over a large number of classes,” in *2008 Sixth Indian Conference on Computer Vision, Graphics & Image Processing*. IEEE, 2008, pp. 722–729.
- [47] O. Vinyals, C. Blundell, T. Lillicrap, D. Wierstra *et al.*, “Matching networks for one shot learning,” in *NeurIPS*, 2016, pp. 3630–3638.
- [48] X. Huang and S. Belongie, “Arbitrary style transfer in real-time with adaptive instance normalization,” in *ICCV*, 2017.
- [49] C. Szegedy, V. Vanhoucke, S. Ioffe, J. Shlens, and Z. Wojna, “Rethinking the inception architecture for computer vision,” in *Proceedings of the IEEE conference on computer vision and pattern recognition*, 2016, pp. 2818–2826.
- [50] R. Zhang, P. Isola, A. A. Efros, E. Shechtman, and O. Wang, “The unreasonable effectiveness of deep features as a perceptual metric,” in *CVPR*, 2018.
- [51] A. Krizhevsky, I. Sutskever, and G. E. Hinton, “Imagenet classification with deep convolutional neural networks,” *Advances in neural information processing systems*, vol. 25, pp. 1097–1105, 2012.
- [52] L. van der Maaten and G. Hinton, “Visualizing data using t-sne,” *Journal of Machine Learning Research*, vol. 9, no. 86, pp. 2579–2605, 2008. [Online]. Available: <http://jmlr.org/papers/v9/vandermaten08a.html>
- [53] H. Talebi and P. Milanfar, “Learned perceptual image enhancement,” in *2018 IEEE international conference on computational photography (ICCP)*. IEEE, 2018, pp. 1–13.
- [54] —, “Nima: Neural image assessment,” *IEEE transactions on image processing*, vol. 27, no. 8, pp. 3998–4011, 2018.
- [55] S. Morozov, A. Voynov, and A. Babenko, “On self-supervised image representations for {gan} evaluation,” in *International Conference on Learning Representations*, 2021. [Online]. Available: <https://openreview.net/forum?id=NeRdBETionN>
- [56] M. Heusel, H. Ramsauer, T. Unterthiner, B. Nessler, and S. Hochreiter, “Gans trained by a two time-scale update rule converge to a local nash equilibrium,” *Advances in neural information processing systems*, vol. 30, 2017.
- [57] D. Bau, J.-Y. Zhu, H. Strobelt, B. Zhou, J. B. Tenenbaum, W. T. Freeman, and A. Torralba, “Gan dissection: Visualizing and understanding generative adversarial networks,” in *Proceedings of the International Conference on Learning Representations (ICLR)*, 2019.
- [58] D. Bau, B. Zhou, A. Khosla, A. Oliva, and A. Torralba, “Network dissection: Quantifying interpretability of deep visual representations,” in *Proceedings of the IEEE conference on computer vision and pattern recognition*, 2017, pp. 6541–6549.
- [59] A. Achille, M. Lam, R. Tewari, A. Ravichandran, S. Maji, C. C. Fowlkes, S. Soatto, and P. Perona, “Task2vec: Task embedding for meta-learning,” in *Proceedings of the IEEE/CVF International Conference on Computer Vision*, 2019, pp. 6430–6439.
- [60] C. Simon, P. Koniusz, R. Nock, and M. Harandi, “On modulating the gradient for meta-learning,” in *European Conference on Computer Vision*. Springer, 2020, pp. 556–572.
- [61] X. Wang and X. Tang, “Face photo-sketch synthesis and recognition,” *IEEE transactions on pattern analysis and machine intelligence*, vol. 31, no. 11, pp. 1955–1967, 2008.
- [62] Y. Wang, A. Gonzalez-Garcia, D. Berga, L. Herranz, F. S. Khan, and J. v. d. Weijer, “Minegan: effective knowledge transfer from gans to target domains with few images,” in *Proceedings of the IEEE/CVF Conference on Computer Vision and Pattern Recognition*, 2020, pp. 9332–9341.
- [63] K. Simonyan, A. Vedaldi, and A. Zisserman, “Deep inside convolutional networks: Visualising image classification models and saliency maps,” *arXiv preprint arXiv:1312.6034*, 2013.
- [64] T. Karras, T. Aila, S. Laine, and J. Lehtinen, “Progressive growing of gans for improved quality, stability, and variation,” *arXiv preprint arXiv:1710.10196*, 2017.
- [65] D. Bau, J.-Y. Zhu, H. Strobelt, B. Zhou, J. B. Tenenbaum, W. T. Freeman, and A. Torralba, “Gan dissection website,” 2019, <https://github.com/CSAILVision/gandissect>.
- [66] S. Zhao, Z. Liu, J. Lin, J.-Y. Zhu, and S. Han, “Differentiable augmentation for data-efficient gan training,” *Advances in Neural Information Processing Systems*, vol. 33, pp. 7559–7570, 2020.
- [67] N. Ruiz, Y. Li, V. Jampani, Y. Pritch, M. Rubinstein, and K. Aberman, “Dreambooth: Fine tuning text-to-image diffusion models for subject-driven generation,” *arXiv preprint arXiv:2208.12242*, 2022.
- [68] K. Chandrasegaran, N.-T. Tran, A. Binder, and N.-M. Cheung, “Discovering Transferable Forensic Features for CNN-generated Images Detection,” in *Proceedings of the European Conference on Computer Vision (ECCV)*, Oct 2022.
- [69] S.-Y. Wang, O. Wang, R. Zhang, A. Owens, and A. A. Efros, “CNN-Generated Images Are Surprisingly Easy to Spot... for Now,” in *IEEE/CVF Conference on Computer Vision and Pattern Recognition (CVPR)*, June 2020.
- [70] K. Chandrasegaran, N.-T. Tran, and N.-M. Cheung, “A Closer Look at Fourier Spectrum Discrepancies for CNN-Generated Images Detection,” in *Proceedings of the IEEE/CVF Conference on Computer Vision and Pattern Recognition (CVPR)*, June 2021, pp. 7200–7209.
- [71] J. Frank, T. Eisenhofer, L. Schönherr, A. Fischer, D. Kolossa, and T. Holz, “Leveraging frequency analysis for deep fake image recognition,” in *International conference on machine learning*. PMLR, 2020, pp. 3247–3258.

- [72] Y. Zhao, T. Pang, C. Du, X. Yang, N.-M. Cheung, and M. Lin, “A recipe for watermarking diffusion models,” *arXiv preprint arXiv:2303.10137*, 2023.
- [73] G. Hinton, O. Vinyals, and J. Dean, “Distilling the knowledge in a neural network,” in *NIPS Deep Learning and Representation Learning Workshop*, 2015. [Online]. Available: <http://arxiv.org/abs/1503.02531>
- [74] K. Chandrasegaran, N.-T. Tran, Y. Zhao, and N.-M. Cheung, “Revisiting Label Smoothing and Knowledge Distillation Compatibility: What was Missing?” in *Proceedings of the 39th International Conference on Machine Learning*, ser. Proceedings of Machine Learning Research, K. Chaudhuri, S. Jegelka, L. Song, C. Szepesvari, G. Niu, and S. Sabato, Eds., vol. 162. PMLR, 17–23 Jul 2022, pp. 2890–2916.
- [75] B. Heo, J. Kim, S. Yun, H. Park, N. Kwak, and J. Y. Choi, “A comprehensive overhaul of feature distillation,” in *Proceedings of the IEEE/CVF International Conference on Computer Vision*, 2019, pp. 1921–1930.
- [76] U. Evci, V. Dumoulin, H. Larochelle, and M. C. Mozer, “Head2toe: Utilizing intermediate representations for better transfer learning,” in *International Conference on Machine Learning*. PMLR, 2022, pp. 6009–6033.
- [77] A. Ramesh, P. Dhariwal, A. Nichol, C. Chu, and M. Chen, “Hierarchical text-conditional image generation with clip latents,” *arXiv preprint arXiv:2204.06125*, 2022.
- [78] R. Gal, Y. Alaluf, Y. Atzmon, O. Patashnik, A. H. Bermano, G. Chechik, and D. Cohen-Or, “An image is worth one word: Personalizing text-to-image generation using textual inversion,” *arXiv preprint arXiv:2208.01618*, 2022.
- [79] H. Li, S. Jialin Pan, S. Wang, and A. C. Kot, “Domain generalization with adversarial feature learning,” in *Proceedings of the IEEE Conference on Computer Vision and Pattern Recognition*, 2018, pp. 5400–5409.
- [80] M. J. Chong and D. Forsyth, “Effectively unbiased fid and inception score and where to find them,” in *Proceedings of the IEEE/CVF conference on computer vision and pattern recognition*, 2020, pp. 6070–6079.
- [81] F. Yu, Y. Zhang, S. Song, A. Seff, and J. Xiao, “Lsun: Construction of a large-scale image dataset using deep learning with humans in the loop,” *arXiv preprint arXiv:1506.03365*, 2015.
- [82] A. Lacoste, A. Luccioni, V. Schmidt, and T. Dandres, “Quantifying the carbon emissions of machine learning,” *arXiv preprint arXiv:1910.09700*, 2019.

SUPPLEMENTARY MATERIAL

This Supplementary Material provides additional experiments, results, analysis and ablation studies to further support our contributions. The Supplementary materials are organized as follows:

CONTENTS

9	Additional Implementation Details of AdAM	19
9.1	Computational overhead	19
9.2	Fisher information approximation using proxy vectors	19
10	Additional Experiment Results	20
10.1	Additional source / target domain adaptation	20
10.2	Visualization of adaptation results with more shots	20
10.3	Additional GAN architectures	20
10.4	KID / Intra-LPIPS / standard deviation of experiments	21
10.5	FID measurements with limited target domain samples	22
10.6	KML induces restrained update of the kernels	23
10.7	Additional Results/Analysis for GAN Dissection	25
11	Additional Discussion	25
11.1	Potential societal impact	25
11.2	Amount of compute	26

REPRODUCIBILITY

We provide [Code](#) to help reproduce the experiments in our work, see our [Project Page](#).

9 ADDITIONAL IMPLEMENTATION DETAILS OF ADAM

9.1 Computational overhead

Our proposed Importance Probing (IP) in AdAM to measure the importance of each individual kernel in the source GAN for the target-domain is lightweight. *i.e.*: proposed IP only requires 8 minutes compared to the adaptation step which requires ≈ 110 minutes (Averaged over 3 runs for FFHQ \rightarrow Cat adaptation experiment). This is achieved through two design choices:

- During IP, only modulation parameters are updated. Given that our modulation design is low-rank KML, the number of trainable parameters is significantly small compared to the actual source GAN. *e.g.*: for the generator, the number of trainable parameters in our proposed IP is only 0.1M whereas the entire generator has 30.1M trainable parameters.
- Our proposed IP is performed for limited number of iterations to measure the importance for the target domain. *i.e.*: IP stage requires only 500 iterations to achieve a good performance for adaptation, while the full adaptation for FSIG may require up to 6000 iterations.

Complete details on number of trainable parameters and compute time for our proposed method and existing FSIG works are provided in Table 8. As one can observe, our proposed AdAM (IP + adaptation) is better than existing FSIG works in terms of trainable parameters and compute time.

TABLE 8: Comparison of training cost in terms of number of trainable parameters, iterations and compute time for different FSIG methods. FFHQ is the source domain and we show results for Babies (top) and Cat (bottom) target domains. One can clearly observe that our proposed IP is extremely lightweight and our KML based adaptation contains much less trainable parameters in the source GAN. All results are measured in containerized environments using a single Tesla V100-SXM2 (32 GB) GPU with batch size of 4. All reported results are averaged over 3 independent runs.

FFHQ \rightarrow Babies				
Method	Stage	# trainable params (M)	# iteration	# time
TGAN [18]	Adaptation	30.1	3000	110 mins
FreezeD [19]	Adaptation	30.1	3000	110 mins
EWC [20]	Adaptation	30.1	3000	110 mins
CDC [16]	Adaptation	30.1	3000	120 mins
DCL [21]	Adaptation	30.1	3000	120 mins
AdAM (Ours)	IP	0.105	500	8 mins
	Adaptation	11.9	1500	45min

FFHQ \rightarrow AFHQ-Cat				
Method	Stage	# trainable params (M)	# iteration	# time
TGAN [18]	Adaptation	30.1	6000	210 mins
FreezeD [19]	Adaptation	30.1	6000	200 mins
EWC [20]	Adaptation	30.1	6000	220 mins
CDC [16]	Adaptation	30.1	6000	300 mins
DCL [21]	Adaptation	30.1	6000	300 mins
AdAM (Ours)	IP	0.105	500	8 mins
	Adaptation	17.85	2500	105 mins

9.2 Fisher information approximation using proxy vectors

Recall in Sec. 4 of main paper, we consider low-rank approximation of modulation matrix using outer product of proxy vectors: $\mathbf{M}_i = \text{reshape}([\mathbf{m}_1^i \mathbf{m}_2^1, \dots, \mathbf{m}_1^i \mathbf{m}_2^{c_{in} \times k \times k}])$, where $|\mathbf{m}_2| = (c_{in} \times k \times k)$. In order to calculate the FI of the modulation matrix, we start with the FI of each element in this matrix. Considering $m_{ij} = \mathbf{m}_1^i \mathbf{m}_2^j$, following equation can be derived by simple application of chain rule of differentiation:

$$\frac{\partial \mathcal{L}}{\partial m_{ij}} = \frac{1}{2\mathbf{m}_2^j} \frac{\partial \mathcal{L}}{\partial \mathbf{m}_1^i} + \frac{1}{2\mathbf{m}_1^i} \frac{\partial \mathcal{L}}{\partial \mathbf{m}_2^j} \quad (4)$$

We use the square of the gradients to estimate the FI [59]. Therefore, the following equation can be obtained between the FI of these variables:

$$\mathcal{F}(m_{ij}) = \frac{1}{4\mathbf{m}_2^{j^2}} \mathcal{F}(\mathbf{m}_1^i) + \frac{1}{4\mathbf{m}_1^{i^2}} \mathcal{F}(\mathbf{m}_2^j) + \frac{1}{2\mathbf{m}_1^i \mathbf{m}_2^j} \frac{\partial \mathcal{L}}{\partial \mathbf{m}_1^i} \frac{\partial \mathcal{L}}{\partial \mathbf{m}_2^j} \quad (5)$$

Then, the FI of the modulation matrix $\mathbf{M}_i = [m_{i1}, m_{i2}, \dots]$, can be calculated as:

$$\begin{aligned}
 \mathcal{F}(\mathbf{M}_i) &= \sum_{j=1}^{|\mathbf{m}_2|} \mathcal{F}(m_{ij}) \\
 &= \sum_{j=1}^{|\mathbf{m}_2|} \left(\frac{1}{4\mathbf{m}_2^{j2}} \mathcal{F}(\mathbf{m}_1^i) + \frac{1}{4\mathbf{m}_1^{i2}} \mathcal{F}(\mathbf{m}_2^j) + \frac{1}{2\mathbf{m}_1^i \mathbf{m}_2^j} \frac{\partial \mathcal{L}}{\partial \mathbf{m}_1^i} \frac{\partial \mathcal{L}}{\partial \mathbf{m}_2^j} \right) \\
 &= \mathcal{F}(\mathbf{m}_1^i) \sum_{j=1}^{|\mathbf{m}_2|} \frac{1}{4\mathbf{m}_2^{j2}} + \frac{1}{4\mathbf{m}_1^{i2}} \sum_{j=1}^{|\mathbf{m}_2|} \mathcal{F}(\mathbf{m}_2^j) \\
 &\quad + \frac{1}{2\mathbf{m}_1^i} \frac{\partial \mathcal{L}}{\partial \mathbf{m}_1^i} \sum_{j=1}^{|\mathbf{m}_2|} \frac{1}{\mathbf{m}_2^j} \frac{\partial \mathcal{L}}{\partial \mathbf{m}_2^j}
 \end{aligned} \tag{6}$$

We empirically observed that discarding (i) the cross-term (ii) the coefficients $(\frac{1}{4\mathbf{m}_2^{j2}}, \frac{1}{4\mathbf{m}_1^{i2}})$ in the importance of each kernel in Eqn. 6 results in a similar FID for the final adapted model. Therefore, the estimation can be simpler and more lightweight. In particular, the following (simpler) estimated version of $\mathcal{F}(\mathbf{M}_i)$ is used in our experiments:

$$\hat{\mathcal{F}}(\mathbf{M}_i) = \mathcal{F}(\mathbf{m}_1^i) + \frac{1}{|\mathbf{m}_2|} \sum_{j=1}^{|\mathbf{m}_2|} \mathcal{F}(\mathbf{m}_2^j) \tag{7}$$

Note that $\hat{\mathcal{F}}(\mathbf{M}_i)$ intuitively estimates the FI of the modulation matrix by a weighted average of its constructing parameters corresponding to their occurrence frequency in calculation of \mathbf{M}_i . We remark that in our implementation, for reporting all of the results in the main paper, and also the additional results in this Supplement, we have used this lightweight estimation Eqn. 7 to calculate the importance of each kernel during importance probing.

10 ADDITIONAL EXPERIMENT RESULTS

10.1 Additional source / target domain adaptation

Proximity analysis. Following [16], we conduct extended experiments using Church as the source domain. [16] uses Haunted houses and Van Gogh Houses as target domains. Similar to Sec. 3 in the main paper, our analysis confirms that these target domains are closer to the source domain (Church). We additionally include palace and yurt as target domains to relax the close proximity assumption. The proximity visualization is shown in Figure 13.

Adaptation results. Besides the results in the main paper, we show complete 10-shot adaptation results for our proposed AdAM for additional source / target domains: Church \rightarrow Haunted House (Figure 14), Church \rightarrow Van Gogh’s House (Figure 15), Church \rightarrow Palace (Figure 16), Church \rightarrow Yurt (Figure 17), FFHQ \rightarrow AFHQ-Dog (Figure 18), FFHQ \rightarrow AFHQ-Wild (Figure 19), FFHQ \rightarrow Sunglasses (Figure 20), FFHQ \rightarrow MetFaces [39] (Figure 21), FFHQ \rightarrow Sketches (Figure 22), FFHQ \rightarrow Amedeo Modigliani’s Paintings (Figure 23), FFHQ \rightarrow Otto Dix’s Paintings (24) and FFHQ \rightarrow Raphael’s Paintings (Figure 25), Cars \rightarrow Wrecked Cars (Figure 26). We also include the comparison to SOTA methods with distant target domains, see FFHQ \rightarrow AFHQ-Dog in Figure 27, FFHQ \rightarrow AFHQ-Wild in Figure 28 and Church \rightarrow Palace in Figure 29. As one can observe, SOTA FSIG methods [16], [20], [21] are unable to adapt well to distant target domains due to *only considering source domain / task in knowledge preservation*. We remark that TGAN [18] suffers severe mode collapse. We clearly show that AdAM (ours) outperforms SOTA FSIG methods [16], [20], [21] and produces high quality images with good diversity.

10.2 Visualization of adaptation results with more shots

In addition to the analysis of increasing the number of shots for target adaptation in Figure 6 and Table 5 in the main paper, here we additionally show the generated images with 100-shot training data, on Babies and AFHQ-Cat as the target domains. FFHQ is the source domain. The results are in Figure 30 where each column represents a fixed noise input. Compared to baseline and SOTA methods, our generated images can still produce the best quality and diversity.

10.3 Additional GAN architectures

We use an additional pre-trained GAN architecture, ProGAN [64], to conduct FSIG experiments for FFHQ \rightarrow Babies, FFHQ \rightarrow Cat, Church \rightarrow Haunted houses and Church \rightarrow Palace setups. For fair comparison, we strictly follow the exact experiment setup discussed in Section 10.1.

Results. The qualitative and quantitative results are in Figures 31 and 32. We remark that the results for FFHQ \rightarrow Babies, FFHQ \rightarrow Cat are included in the main paper, see Sec. 6.7. As one can observe, our proposed method consistently outperforms other baseline and

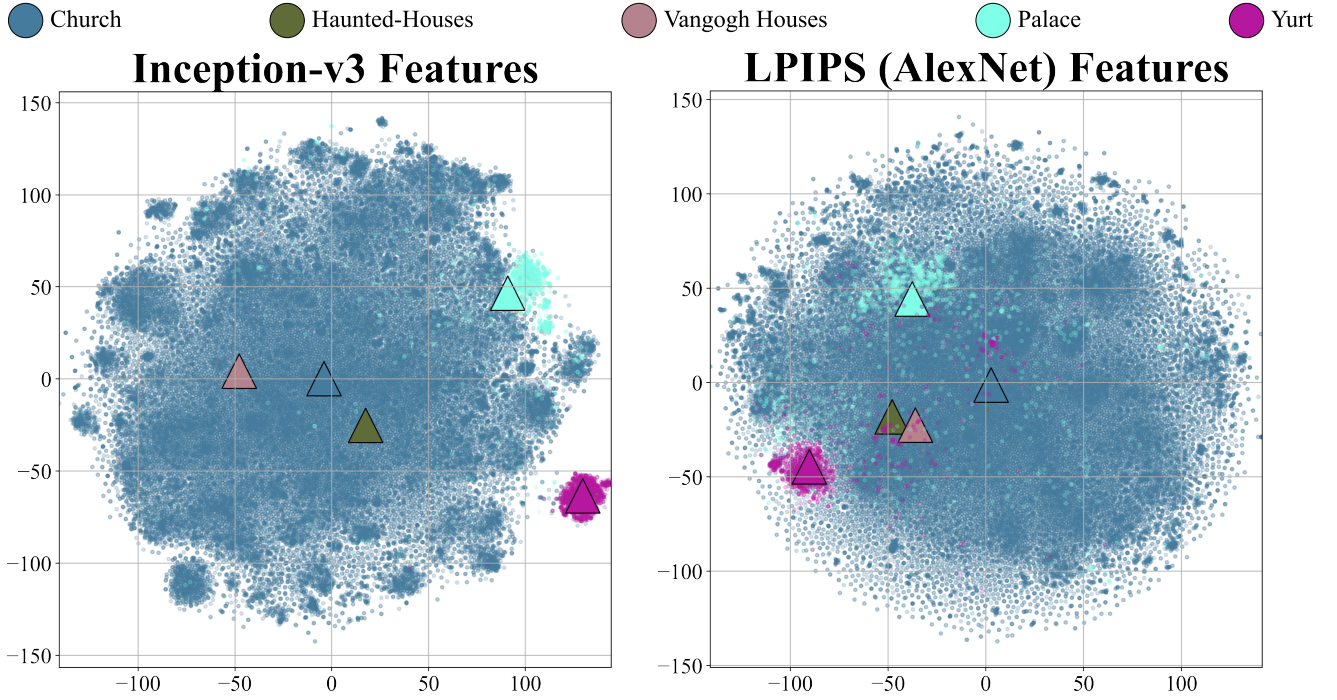


Fig. 13: *Source-target domain proximity Visualization*: We use Church as the source domain following [16]. We show source-target domain proximity by visualizing Inception-v3 (Left) [49] and LPIPS (Middle) [50] –using AlexNet [51] backbone– features, and quantitatively using FID / LPIPS metrics (Right). For feature visualization, we use t-SNE [52] and show centroids (\triangle) for all domains. FID / LPIPS is measured with respect to FFHQ. There are 2 important observations: ① Common target domains used in existing FSIG works (Haunted Houses, Van Gogh Houses) are notably proximal to the source domain (Church). This can be observed from the feature visualization and verified by FID / LPIPS measurements. ② We clearly show using feature visualizations and FID / LPIPS measurements that additional setups – Palace [13] and Yurt [13] – represent target domains that are distant from the source domain (Church). We remark that due to availability of only 10-shot samples in the target domain, FID / LPIPS are not measured in these setups.



Fig. 14: Church \rightarrow Haunted House

SOTA FSIG methods with another pre-trained GAN model (ProGAN [64]), demonstrating the effectiveness and generalizability of our method over various GAN architectures.

10.4 KID / Intra-LPIPS / standard deviation of experiments

KID / Intra-LPIPS. In addition to FID scores reported in the main paper, we evaluate KID [79] and Intra-LPIPS [50]. We remark the KID (\downarrow) is another metric in addition to FID (\downarrow) to measure the quality of generated samples, and Intra-LPIPS (\uparrow) measures the diversity of generated samples. In literature, the original LPIPS [50] evaluates the perceptual distance between images. We follow CDC [16] and DCL [21] to measure the Intra-LPIPS, a variant of LPIPS, to evaluate the degree of diversity. Firstly, we generate 5,000 images and assign them to one of 10-shot target samples, based on the closet LPIPS distance. Then, we calculate the LPIPS of 10 clusters and take

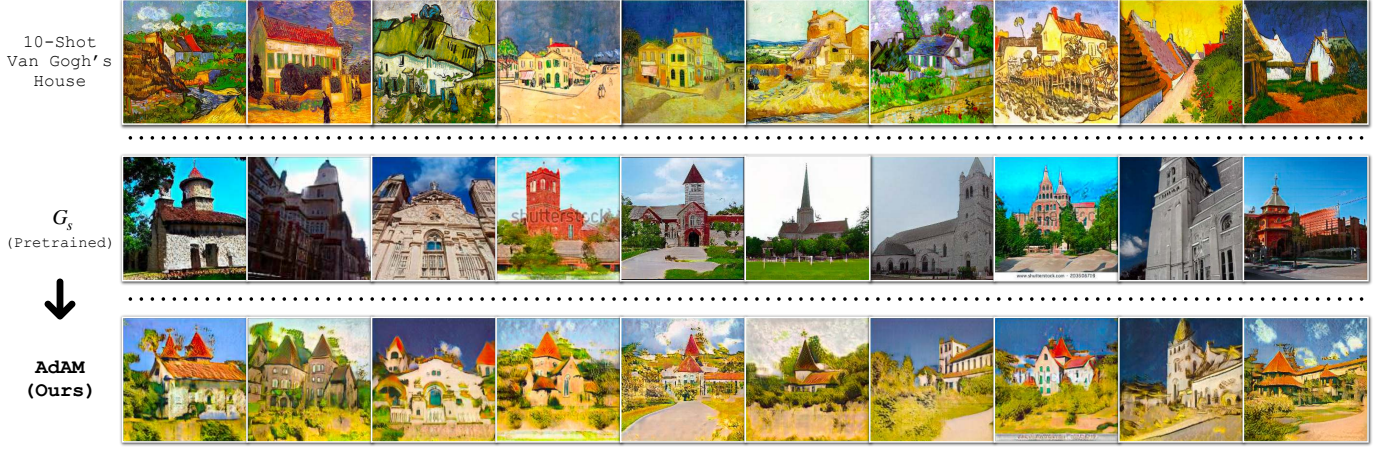


Fig. 15: Church → Van Gogh's House



Fig. 16: Church → Palace (distant domain)

average. KID and Intra-LPIPS results are reported in Tables 9 and 10 respectively. As one can observe, our proposed adaptation-aware FSIG method outperforms SOTA FSIG methods [16], [20], [21] and produces high quality images with good diversity.

TABLE 9: KID (\downarrow) score of different methods with the same checkpoint of Table 2 in the main paper. The values are in 10^3 units, following [12], [39].

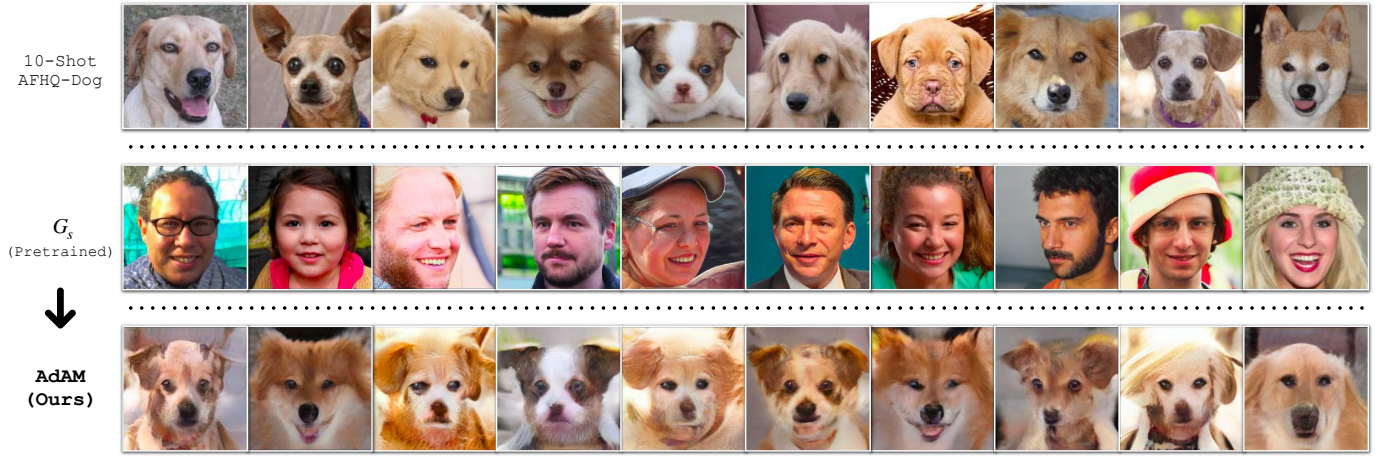
Method	TGAN	FreezeD	EWC	CDC	DCL	RSSA	LLN	AdAM
Babies	81.92	65.14	51.81	51.74	43.46	73.99	39.42	28.38
AFHQ-Cat	41.912	38.834	58.65	196.60	117.82	247.6	267.62	32.78

TABLE 10: Intra-LPIPS (\uparrow) of different methods, the standard deviation is calculated over 10 clusters. Compared to the baseline models (TGAN/FreezeD) or state-of-the-art FSIG methods (EWC/CDC/DCL/RSSA/LLN), our proposed method can achieve a good trade-off between diversity and quality of the generated images, see Table 2 in main paper for FID score.

Method	TGAN	FreezeD	EWC	CDC	DCL	RSSA	LLN	AdAM
Babies	0.517 ± 0.03	0.518 ± 0.06	0.523 ± 0.03	0.573 ± 0.04	0.582 ± 0.03	0.577 ± 0.03	0.585 ± 0.02	0.590 ± 0.03
AFHQ-Cat	0.490 ± 0.02	0.492 ± 0.04	0.587 ± 0.04	0.629 ± 0.03	0.616 ± 0.05	0.618 ± 0.03	0.630 ± 0.04	0.557 ± 0.02

10.5 FID measurements with limited target domain samples

To characterize source \rightarrow target domain proximity, we used FID and LPIPS measurements in Sec. 3 in the main paper. FID involves distribution estimation using first-order (mean) and second-order (trace) moments, i.e.: $\text{FID} = \text{mean}_{\text{component}} + \text{trace}_{\text{component}}$ [56]. Generally, 50K real and generated samples are used for FID calculation [80]. Given that some of our target domain datasets contain

Fig. 17: Church \rightarrow Yurt (distant domain)Fig. 18: FFHQ \rightarrow AFHQ-Dog (distant domain)

limited samples, e.g.:AFHQ Cat [5], Dog [5], Wild [5] datasets contain $\approx 5K$ samples, we conduct extensive experiments to show that FID measurements with limited samples give reliable estimates, thereby reliably characterizing source \rightarrow target domain proximity. Specifically, we decompose FID into mean and trace components and study the effect of target domain sample size to show that our proximity measurements using FID are reliable.

Experiment setup. We use 3 large datasets namely FFHQ [3] (70K samples), LSUN-Bedroom [81] (70K samples) and LSUN-Cat [81] (70K samples). We use FFHQ (70K samples) as the source domain and study the effect of sample size on FID measure. Specifically, we decompose FID into mean and trace components in this study. We consider FFHQ (self-measurement), LSUN-Bedroom and LSUN-cat as target domains. We sample 13, 130, 1300, 2600, 5200, 13000, 52000 samples from the target domain and measure the FID with FFHQ (70K samples), and compare it against the FID obtained by using the entire 70K samples from the target domain.

Results / Analysis. The results are shown in Table 11. As one can observe, with ≈ 2600 samples, we can reliably estimate FID as it becomes closer to the FID measured using the entire 70K target domain samples. Hence, we show that our source \rightarrow target proximity measurements using FID are reliable.

10.6 KML induces restrained update of the kernels

Recall that for a convolutional kernel that we applied KML, we use Eqn 1 in the main paper to modulate its parameters for the knowledge preservation, where we only update the modulation parameters and keep the pretrained weights fixed. In our experiments, we have demonstrated that KML can preserve source knowledge that is useful for target domain adaptation. In this section, we demonstrate that, our proposed KML in AdAM indeed achieves restrained update of the important kernels, therefore it leads to the effective knowledge preservation (more implementation details of KML are in Sec. 4 of the main paper).

Experiment setups. We compute the percentage of weights \mathbf{W} update (normalized), take average over all kernels and layers, and compare with three types of training scheme: simple fine-tuning, KML to all kernels in the GAN, and our proposed AdAM with a threshold to determine if a kernel should be modulated. The output is a single scalar q (i.e., percentage) as below:

$$q\% = \Delta \mathbf{W} / \|\mathbf{W}\| \times 100\%, \quad (8)$$

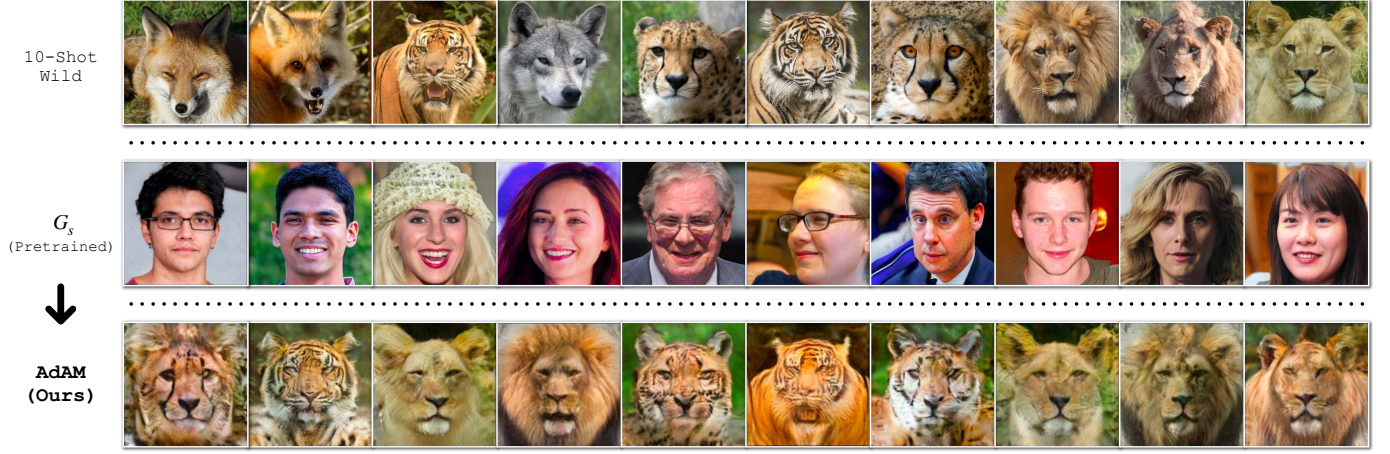


Fig. 19: FFHQ → AFHQ-Wild (distant domain)



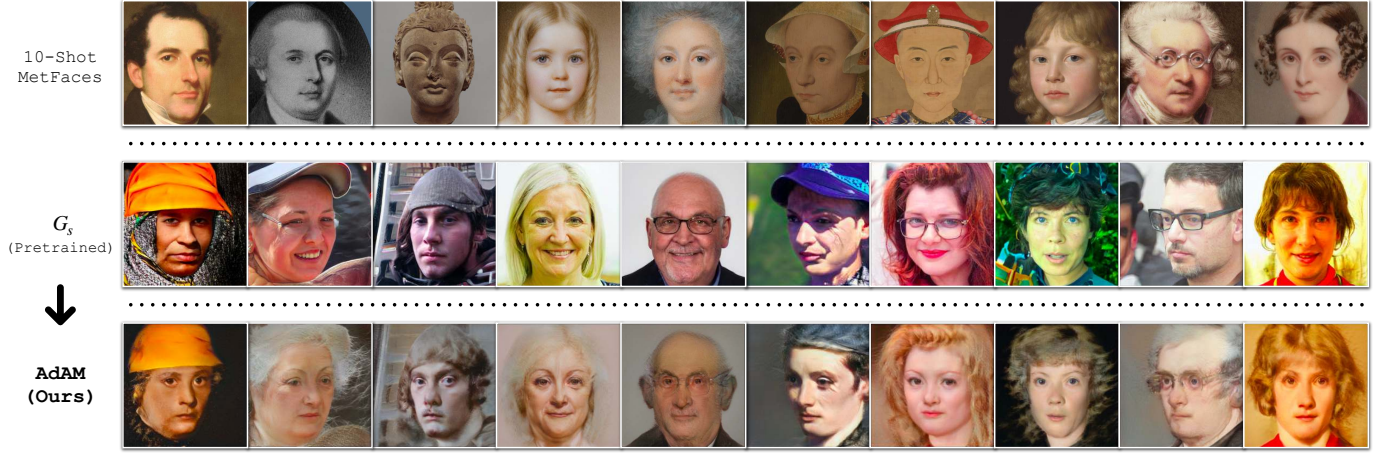
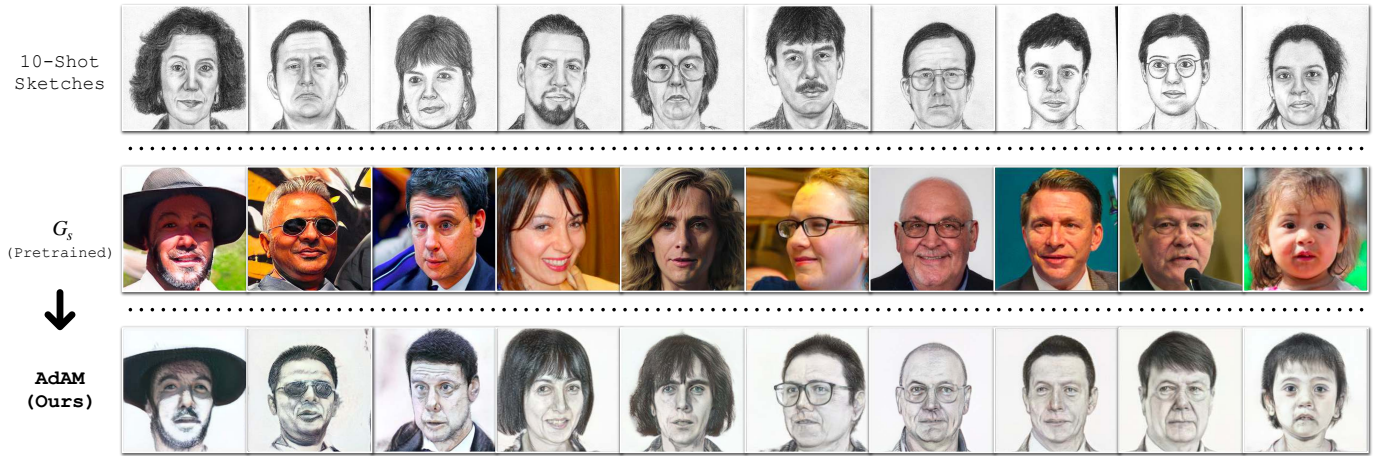
Fig. 20: FFHQ → Sunglasses

TABLE 11: *FID measurements with limited target domain samples give reliable estimates to characterize source → target domain proximity*: FFHQ (70K) is the source domain. We use FFHQ (self-measurement), LSUN-Bedroom and LSUN-Cat as target domains. We use different number of samples from target domain to measure FID. We also decompose FID into mean and trace components in this study. We sample 13, 130, 1300, 2600, 5200, 13000, 52000 images from the target domain and measure the FID with source domain (FFHQ / 70K), and compare it against the FID obtained by using the entire 70K samples from the target domain. Each experiment is repeated *100 times* and we report the results with standard deviation. We also report mean and trace components separately. As one can observe, with ≈ 2600 samples, we can reliably estimate FID as it becomes closer to the FID measured using the entire 70K target domain samples. Therefore, this study shows that our source → target proximity measurements using FID are reliable.

FID		13	130	1300	2600	5200	13, 000	52, 000	70, 000
FFHQ	FID	196.3 ± 11.8	83.4 ± 2.2	15.3 ± 0.2	7 ± 0.1	3.3 ± 0	1.2 ± 0	0.1 ± 0	0 ± 0
	mean	12 ± 2.7	1.3 ± 0.3	0.1 ± 0	0.1 ± 0	0 ± 0	0 ± 0	0 ± 0	0 ± 0
	trace	184.3 ± 10.3	82.2 ± 2	15.2 ± 0.2	6.9 ± 0.1	3.3 ± 0	1.1 ± 0	0.1 ± 0	0 ± 0
Bedroom	FID	358.5 ± 9.3	301.9 ± 2.4	251 ± 1.2	243.6 ± 0.8	240.1 ± 0.5	238.2 ± 0.4	237.2 ± 0.2	237.2 ± 0.1
	mean	139.3 ± 8	131.8 ± 2.5	131.4 ± 0.9	131.1 ± 0.6	131.1 ± 0.4	131.1 ± 0.3	131.1 ± 0.1	131.1 ± 0.1
	trace	219.1 ± 9.9	170.1 ± 1.9	119.6 ± 0.6	112.5 ± 0.4	109.1 ± 0.3	107.1 ± 0.2	106.1 ± 0.1	106 ± 0.1
Cat	FID	370.2 ± 18.7	283.7 ± 4.4	209.7 ± 1.2	199.9 ± 0.8	195.3 ± 0.6	192.8 ± 0.4	191.4 ± 0.2	191.3 ± 0.1
	mean	105.7 ± 8.4	93 ± 2.2	91.7 ± 0.8	91.7 ± 0.5	91.6 ± 0.4	91.6 ± 0.2	91.6 ± 0.1	91.6 ± 0.1
	trace	264.5 ± 15.7	190.7 ± 3.6	118 ± 0.9	108.2 ± 0.6	103.7 ± 0.4	101.2 ± 0.3	99.9 ± 0.1	99.7 ± 0.1

where $\Delta \mathbf{W} = |\hat{\mathbf{W}} - \mathbf{W}|$ and $\hat{\mathbf{W}}$ is obtained in Eqn 1 in the main paper (note that in AdAM only part of the kernels are updated). For the source/target domains, we apply FFHQ → Babies and FFHQ → AFHQ-Cat, similar to the experiments in Table 2 in the main paper.

Results and analysis. The results are shown in Table 12. We demonstrate that, indeed the proposed KML can achieve restrained update of kernels that is updated, therefore the source knowledge important for target domain adaptation is effectiveness preserved.

Fig. 21: FFHQ \rightarrow MetFacesFig. 22: FFHQ \rightarrow Sketches

10.7 Additional Results/Analysis for GAN Dissection

In this section, we provide additional GAN dissection results as a way to interpret and visualize the knowledge / information encoded by high FI kernels (identified by our proposed AdAM for FSIG) that are important for target domain adaptation:

- Visualizing high FI kernels for Church \rightarrow Haunted Houses adaptation : The results for FI estimation for kernels and several distinct semantic concepts learnt by high FI kernels are shown in Figure 33. In Figure 33, we visualize four examples of high FI kernels: (a), (b), (c), (d) corresponding to concepts building, building, tree and wood respectively. Using GAN Dissection, we observe that a notable amount of high FI kernels correspond to useful source domain concepts including building, tree and wood (texture) which are preserved when adapting to Haunted Houses target domain. We remark that these preserved concepts are useful to the target domain for adaptation.
- Visualizing high FI kernels for Church \rightarrow Palace adaptation : The results for FI estimation for kernels and several distinct semantic concepts learnt by high FI kernels are shown in Figure 34. In Figure 34, we visualize four examples of high FI kernels: (a), (b), (c), (d) corresponding to concepts grass, grass, building and building respectively. Using GAN Dissection, we observe that a notable amount of high FI kernels correspond to useful source domain concepts including grass and building which are preserved when adapting to Palace target domain. We remark that these preserved concepts are useful to the target domain (Palace) for adaptation.

11 ADDITIONAL DISCUSSION

11.1 Potential societal impact

Given very limited target domain samples (i.e.: 10-shot or less), our proposed method achieves SOTA results in FSIG with different source / target domain proximity. In the main paper, we discussed the ethical concern by adapting our FSIG method to a particular person (we used Obama Dataset). Here, we show additional adaptation results (1-shot, 5-shot and 10-shot), as shown in Figure 35. Though our work shows exciting results by pushing the limits of FSIG, we urge researchers, practitioners and developers to use our work with privacy, ethical and moral concerns.

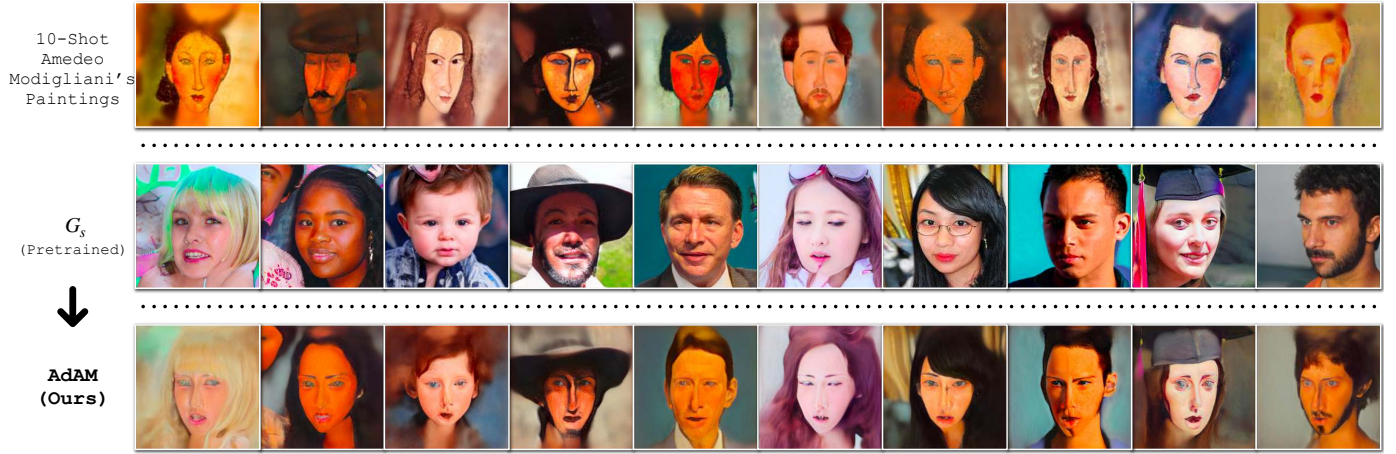


Fig. 23: FFHQ → Amedeo Modigliani's Paintings

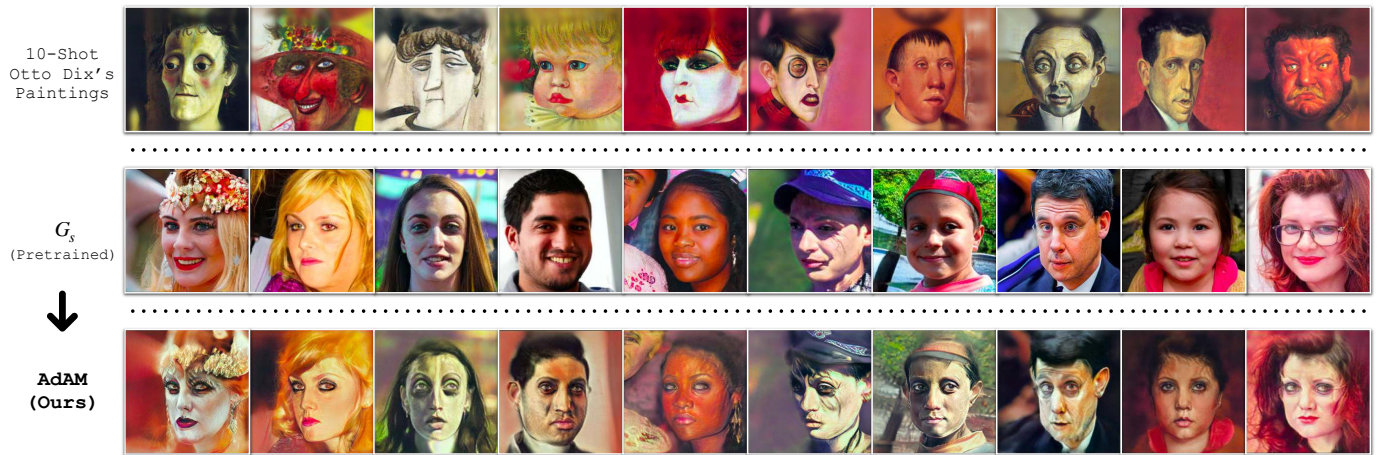


Fig. 24: FFHQ → Otto Dix's Paintings

11.2 Amount of compute

The amount of computation consumed in this work is reported in Table 13. We include the compute amount for each experiment as well as the CO₂ emission (in kg). In practice, our experiments can be run on a single GPU and each experiment can be finished in 2 hours, therefore, the computational demand of our work is not high.

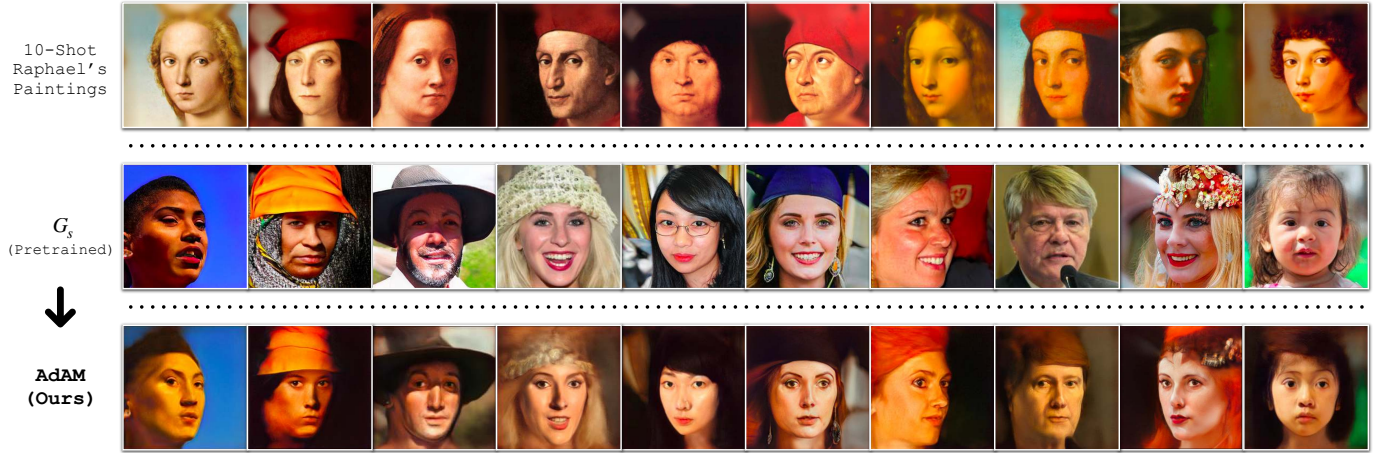


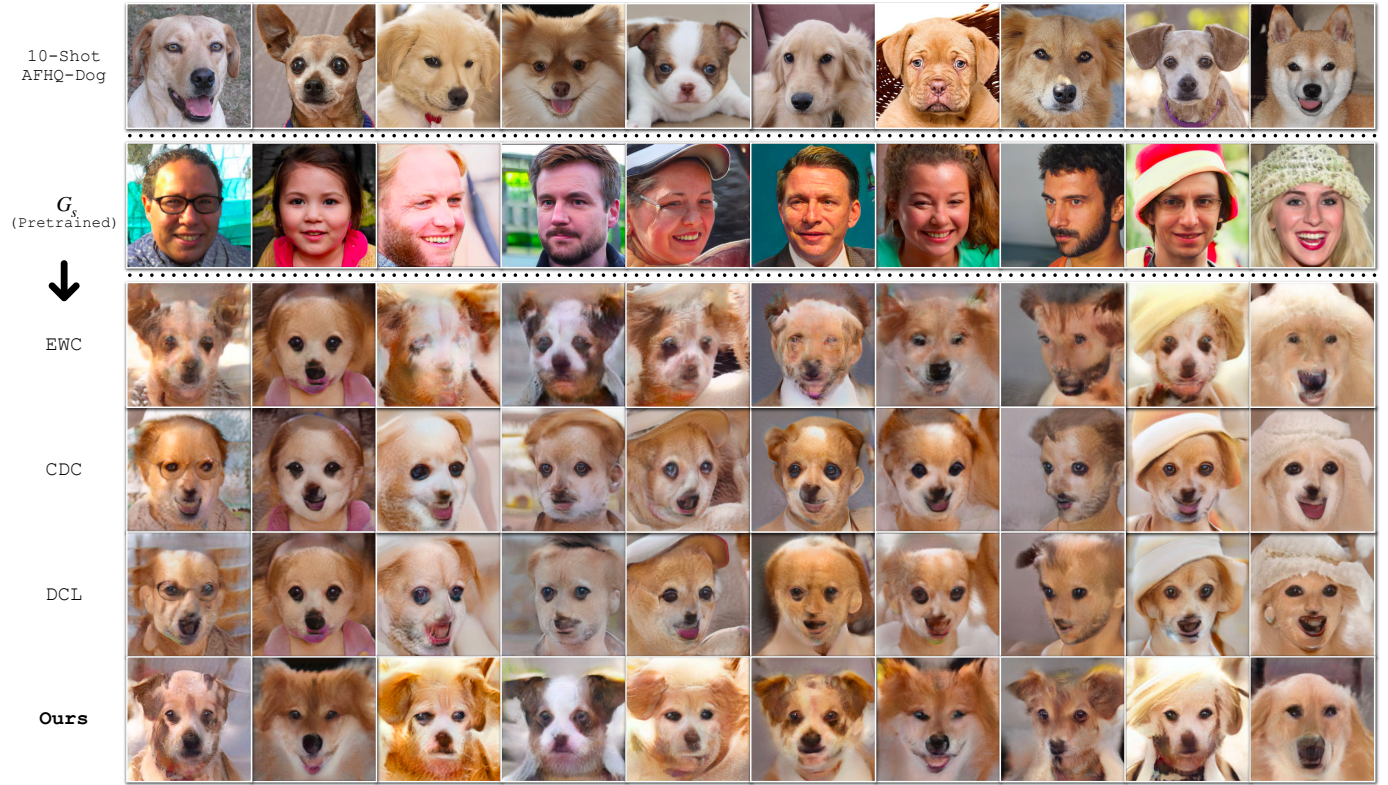
Fig. 25: FFHQ → Raphael's Paintings

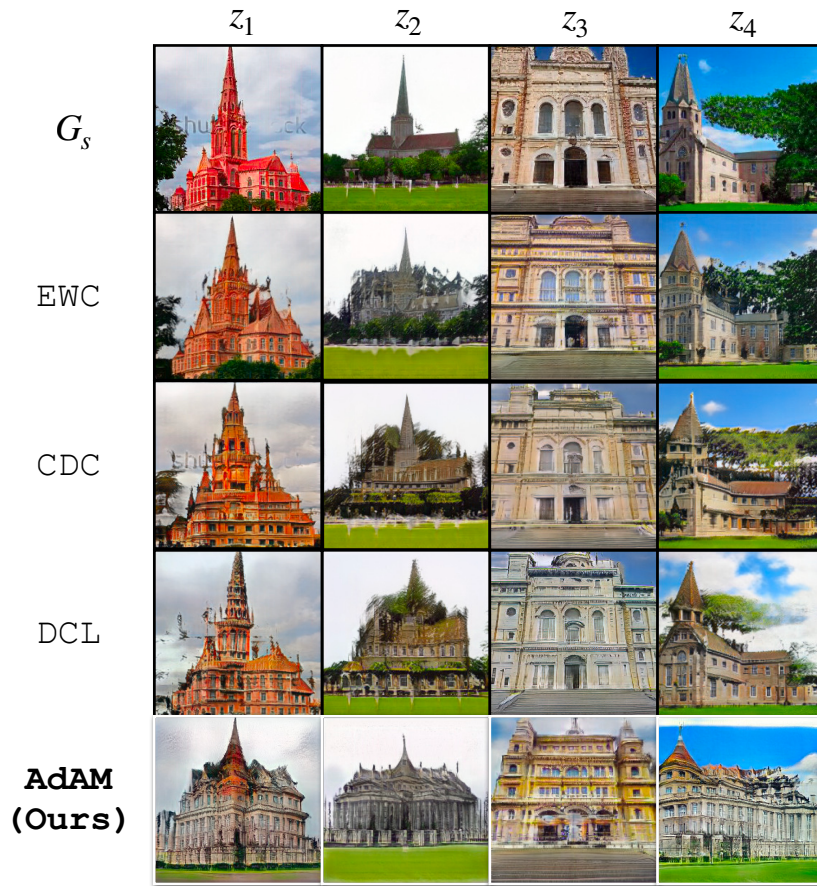
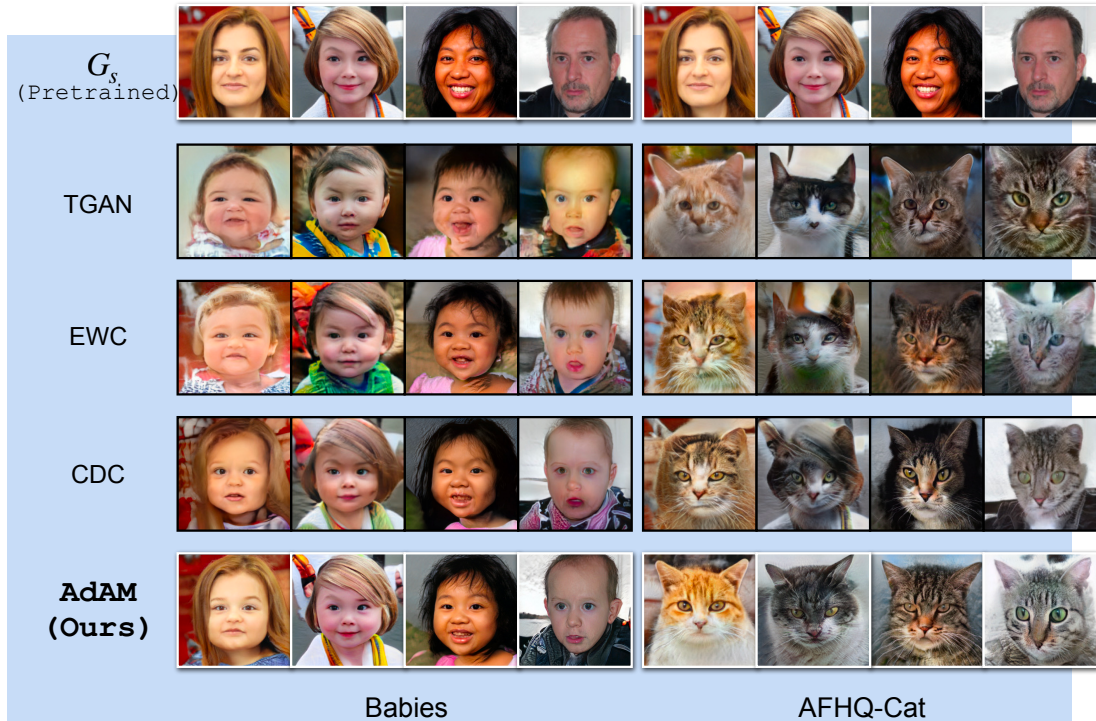


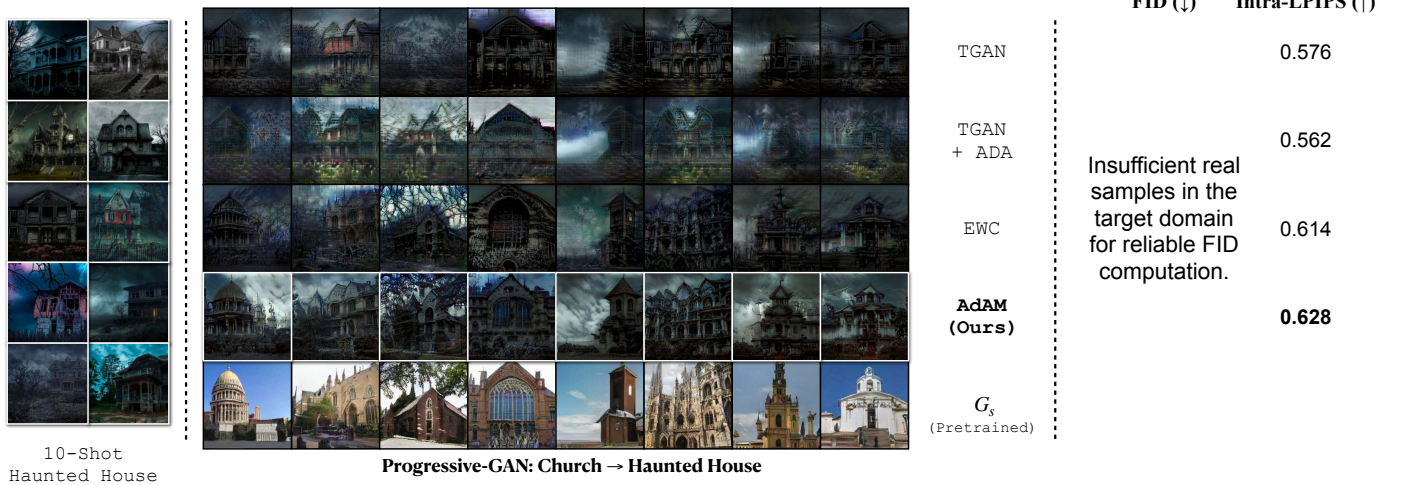
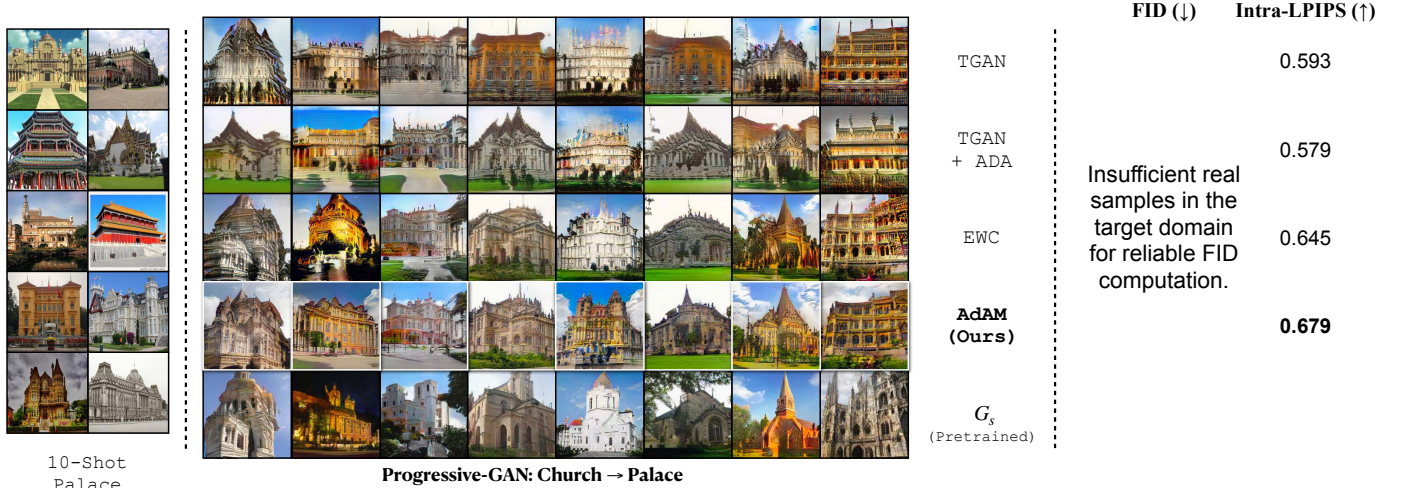
Fig. 26: Cars → Wrecked Cars

TABLE 12: Percentage change of weights before and after the target domain adaptation. It is clearly observed that, our proposed KML indeed achieves restrained updated to individual kernels, and consequently the source knowledge identified important for target domain is effectively preserved. This is also validated through various visualization results in our experiments.

FFHQ → Babies		
Method	Generator	Discriminator
TGAN [18]	35.83%	46.76%
AdAM (apply KML to all kenrels)	2.62 %	2.28%
AdAM (Ours, apply KML to partial kernels)	19.03%	20.32%
FFHQ → AFHQ-Cat		
Method	Generator	Discriminator
TGAN [18]	50.48%	73.34%
AdAM (apply KML to all kenrels)	7.28%	4.80%
AdAM (Ours, apply KML to partial kernels)	35.64 %	32.99%

Fig. 27: Comparison to SOTA methods on FFHQ \rightarrow AFHQ-Dog.Fig. 28: Comparison to SOTA methods on FFHQ \rightarrow AFHQ-Wild.

Fig. 29: Church \rightarrow Palace (distant domain)Fig. 30: FFHQ \rightarrow Babies (Left) and AFHQ-Cat (Right) with 100 samples for adaptation.

Fig. 31: Church \rightarrow Haunted Houses adaptation results using pre-trained ProGAN [64] generator.Fig. 32: Church \rightarrow Palace adaptation results using pre-trained ProGAN [64] generator.

Visualizing the Importance Probing Results using GAN Dissection

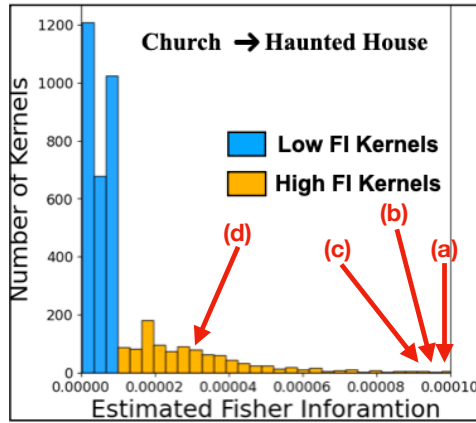


Fig. 33: Visualizing high FI kernels using GAN Dissection [57] for Church → Haunted Houses 10-shot adaptation. In visualization of each high FI kernel, the first row shows different images generated by the source generator, and the second row highlights the concept encoded by the corresponding high FI kernel as determined by GAN Dissection. We observe that a notable amount of high FI kernels correspond to useful source domain concepts including building (a, b), tree (c) and wood (d) which are preserved when adapting to Haunted Houses target domain. We remark that these preserved concepts are useful to the target domain (Haunted House) for adaptation.

Visualizing the Importance Probing Results using GAN Dissection

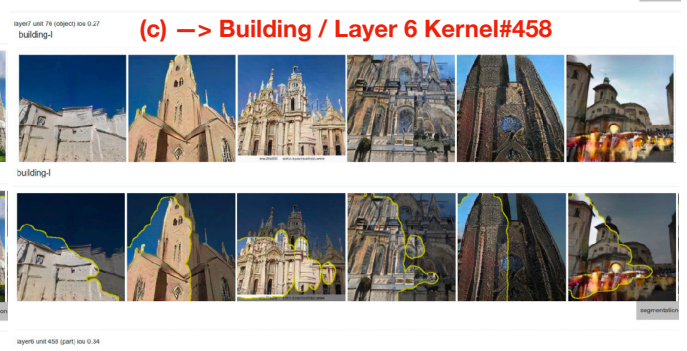
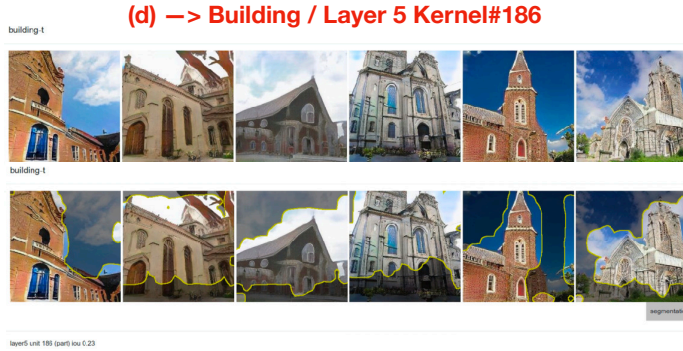
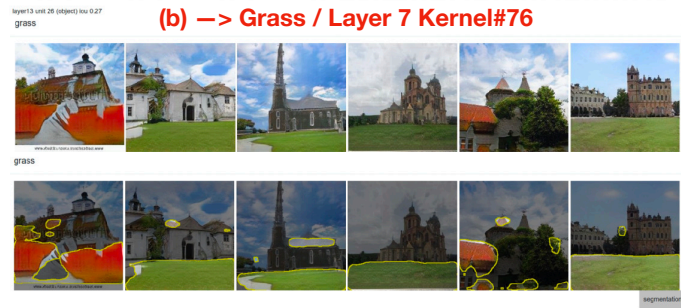
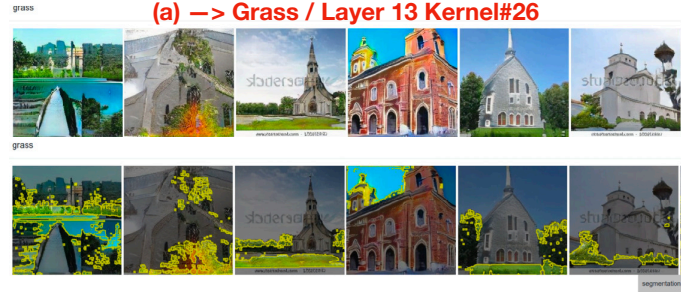
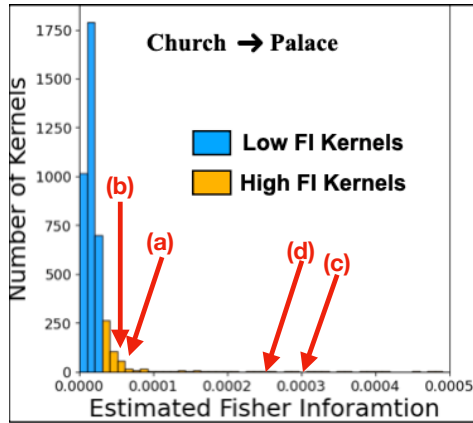


Fig. 34: Visualizing high FI kernels using GAN Dissection [57] for Church → Palace 10-shot adaptation. In visualization of each high FI kernel, the first row shows different images generated by the source generator, and the second row highlights the concept encoded by the corresponding high FI kernel as determined by GAN Dissection. We observe that a notable amount of high FI kernels correspond to useful source domain concepts including grass (a, b) and building (c, d) which are preserved when adapting to Palace target domain. We remark that these preserved concepts are useful to the target domain (palace) for adaptation.



Fig. 35: Complete results for FFHQ → Obama Dataset adaptation.

TABLE 13: The GPU hours consumed for the experiments conducted to obtain the reported values. CO₂ emission values are computed using <https://mlco2.github.io/impact> [82]. We remark since we mostly use the pretrained models in our experiments, therefore, our algorithm is friendly to individual practitioners.

Experiment	Hardware Platform	GPU hours	Carbon emitted in kg
Main paper : Table 2	Tesla V100-SXM2 (32 GB)	306	52.33
Main paper : Table 3		48	8.21
Main paper : Table 4		15	2.56
Main paper : Table 5		183	31.29
Main paper : Table 6		48	8.21
Main paper : Table 7		31	5.30
Main paper : Figure 2		6	1.03
Main paper : Figure 3 / Figure 5		120	20.52
Main paper : Figure 6		40	6.84
Main paper : Figure 7		22	3.76
Main paper : Figure 8		210	35.91
Main paper : Figure 9		120	20.52
Main paper : Figure 10		12	2.05
Main paper : Figure 11		34	5.81
Main paper : Figure 12		2	0.34
Supplement : Extended Experiments	Tesla V100-SXM2 (32 GB)	86	14.71
Supplement : Ablation Study		32	5.47
Hyper-parameter tuning	Tesla V100-SXM2 (32 GB)	30	5.13
Total	-	1345	229.99